Supporting Information

Induced *fac–mer* rearrangements in $\{M(CO)_3\}^+$ complexes (M = Re, $^{99(m)}$Tc) by a PNP ligand

Manuel Luca Besmer,*[a] Flurina Schwitter,[a] Federica Battistin,[a] Henrik Braband,[a] Thomas Fox,[a] Bernhard Spingler[a] and Roger Alberto[a]

[a]Department of Chemistry, University of Zurich, Winterthurerstrasse 190, CH-8057 Zurich, Switzerland

E-mail: manuel.besmer@chem.uzh.ch

Table of Contents

1 General Experimental Details

Materials: *Unless* otherwise stated, all chemicals were of reagent grade or higher, obtained from commercial sources and used without further purification. Solvents for reactions were of *p.a.* grade or distilled prior to their use. Deuterated NMR-solvents were purchased from *Armar Chemicals* (CH) or *Cambridge Isotope Laboratories, Inc.* (UK). $(NH_4)[^{99}TcO_4]$ was purchased from *Oak Ridge* and treated with H_2O_2 prior to reactions for re-oxidation. $[^{99m}Tc(H_2O)_3(CO)_3]^+$ ($[\mathbf{6}]^+$) was synthesized with the *isolink kit* chemicals sodium boranocarbonate, sodium tartrate dihydrate and sodium tetraborate decahydrate.[1,2] $(NEt_4)_2[Re(CO)_3Br_3]$, $(NEt_4)_2[Tc(CO)_3Cl_3]$ and 2,6-bis((di-tertbutylphosphino)methyl) pyridine ($^{Pyr}PNP^{tBu}$) were synthesized following literature procedures.[3–5] $Na[^{99m}TcO_4]$ in 0.9% saline was eluted from a $^{99}Mo/^{99m}Tc$ *Ultratechnekow FM* generator purchased from *b. e. imaging* AG (Switzerland). Caution: ^{99}Tc is a weak β-emitter, ^{99m}Tc is a weak γ-emitter. All experiments must be carried out in licensed and appropriately shielded laboratories for low-level radioactive materials. **NMR:** NMR spectra were recorded in deuterated solvents at 298 K on *Bruker AV-400* (400 MHz) or *Bruker AV2-500* (500 MHz) spectrometers. ^1H and ^{13}C chemical shifts (δ) are given in ppm relative to residual solvent resonances (CD_2Cl_2 ^1H: δ 5.32; ^{13}C: δ 53.84; THF-d_8: ^1H: δ 1.72; ^{13}C: δ 25.31). Signal assignments are based on coupling constants and/or supportive NMR experiments. The NMR measurements were highly influenced by the characteristics of technetium. Its paramagnetic nature and the large nuclear quadrupolar moment both strongly accelerate t_1 and t_2 relaxation up to complete signal extinction. **IR:** FT-IR spectra were recorded with *SpectrumTwo FT-IR Spectrometer* (*Perkin–Elmer*) and samples were applied as KBr pellets. **LSC: Technetium content measurements:** Products were dissolved in the appropriate solvents. The measurements were carried out with a scintillation cocktail (Packard Ultimate Gold XR) and a *Hidex 300 SL* liquid scintillation counter. Yields of compounds were calculated from activity yields by LSC measurement. **Microwave reactions:** Microwave assisted reactions (^{99m}Tc) were carried out in a *Biotage Initiator*. **X-ray diffraction:** Single-crystal X-ray diffraction data was collected at 160(1) K on a *Rigaku OD XtaLAB Synergy*, Dualflex, *Pilatus 200K* diffractometer using a single wavelength X-ray source (Cu K_α radiation: λ = 1.54184 Å for ([**3**](PF_6), [**3**](BF_4), [**5**](PF_6), **9**) or on a *Rigaku XtaLAB Synergy*, Dualflex, *HyPix* diffractometer using a single wavelength X-ray source (Cu K_α radiation: λ = 1.54184 Å for (**2**) or Mo K_α radiation: λ = 0.71073 Å for **11**) from a micro-focus sealed X-ray tube and an *Oxford* liquid-nitrogen *Cryostream* cooler. The selected suitable single crystal was mounted using polybutene oil on a flexible loop fixed on a goniometer head and immediately transferred to the diffractometer. Pre-experiments, data collection, data reduction and analytical absorption correction[6] were performed with the program suite *CrysAlis^{Pro}*.[7] Using *Olex2*,[8] the structures were solved with the *SHELXT*[9] small molecule structure solution program and refined with the *SHELXL 2018/3*[10] program package by full-matrix least-squares minimization on F^2. *PLATON*[11] was used to check the result of the X-ray analysis. Ill-defined electron density in [**9**] had to be treated with the *SQUEEZE* procedure in PLATON.[11] For more details about the data collection and refinement parameter, see the CIF files. **UHPLC-ESI-MS:** Samples (2 µl injection) were analyzed with a *Vanquish™ Horizon UHPLC* System (*Thermo Fisher Scientific*, Waltham, USA) connected to a *Vanquish™* eλ detector and ISQ-EM ESI mass spectrometer (*Thermo Fisher Scientific*, Waltham, USA), operated in positive mode; scan range m/z 200–1500. Separation was performed with an *Acquity BEH C18* HPLC column (1.7 µm particle size, 2x100 mm, Waters) kept at 40 °C. The mobile phase consisted of A: H_2O + 0.1% HCOOH and B: CH_3CN + 0.1% HCOOH. UV spectra were recorded between 190 and 670 nm at a 4 nm resolution and at 5 Hz. The mass spectrometer was operated in the positive (negative) electrospray ionization mode at 3000 V (-2'000 V) capillary voltage with a N_2 Sheath gas pressure of 41.9 psi, auxiliar gas pressure of 5.5 psi and sweep gas pressure of 0.1 psi. Spectra were acquired in the mass range from m/z 150 to 2'000. Method: 0-0.5 min 5% B; 0.5-4.5 min linear gradient from 5 to 100% B; 4.5-5 min 100% B, 5-5.1 min linear gradient from 100 to 5% B, 5.1-5.5 min isocratic gradient with 5% B; flow rate was 0.6 mL/min. **Radio-HPLC:** VWR Hitachi Chromaster with tuneable UV detector (250nm), radio detector (Berthold LB514, YG 150-S5D), Nucleosil C-18 column (100Å, 5µm, 250×4mm), flow rate of 0.5mL/min, 0.1% TFA in H_2O (solvent A) and methanol (solvent B) with the following gradient: 0-3min: 90% A (10% B); 3-3.1min: 90% A

(10% B) to 75% A (25% B); 3.1–9min: 75% A (25% B); 9-9.1min: 75% A (25% B) to 66% A (34% B); 9.1-20min: 66% A (34% B) to 0% A (100% B); 20-25min: 0% A (100% B); 25-30min: 0% A (100% B) to 90% A (10% B).

2. Remarks on NMR spectroscopy with ^{99}Tc complexes

We have already reported on analogous observations with ^{99}Tc NMR spectroscopy that are true for this work as well, as described below.[12] The influence of quadrupolar nuclei like ^{99}Tc (spin I = 9/2, quadrupole relaxation time T_{1Q}) onto the relaxation time of scalarly coupled nuclei like ^{13}C ($T_{1\text{-}SC}$) is described by formula (I) according to literature.[13]

$$\frac{1}{T_{1-SC}} = \frac{8\pi^2 J^2}{3} I(I+1) \frac{T_{1Q}}{1+(\omega_C - \omega_I)^2 T_{1Q}^2} \quad \text{(I)}$$

In this regard, a significant increase of ^{13}C T_1 relaxation due to strong scalar coupling with ^{99}Tc might be an explanation for the unobservability of carbon sites which are directly bound to the technetium center (CO):

Considering ^{13}C-^{99}Tc coupling constants J of some 100 Hz and a typical ^{99}Tc relaxation time T_{1Q} in the *millisecond* range, in conjunction with the close resonance frequencies of carbon and technetium (125 vs. 113 MHz), relation (I) predicts significant scalar ^{13}C relaxation $1/T_{1\text{-}SC}$ in the kHz range, causing broadening and weakening effects onto the ^{13}C signal, up to its loss.

Rhenium bound ^{13}C nuclei are, in contrast, *not* influenced by scalar T_1 relaxation as both rhenium isotopes (^{185,187}Re) undergo extraordinarily fast quadrupolar relaxation T_{1Q} in the *microsecond* range. Therefore, equation (I) yields values close to zero, cancelling any scalar relaxation effects $1/T_{1\text{-}SC}$ in the case of rhenium.

3 Experimental Procedures and Data

3.1 *mer*–[Re(^{Pyr}PNP^{tBu})(CO)$_3$]$^+$, [3](PF$_6$)

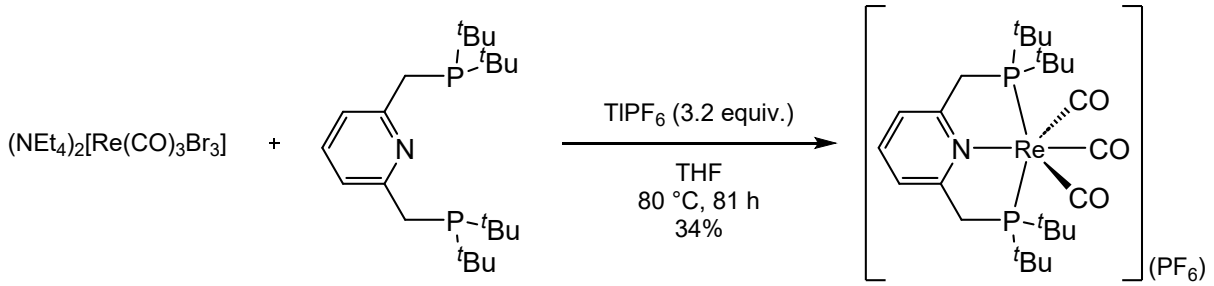

(NEt$_4$)$_2$[**1**] **2** [**3**](PF$_6$)

Synthesis: A round-bottom flask was charged with (NEt$_4$)$_2$[**1**] (100.0 mg, 129.0 µmol), ^{Pyr}PNP^{tBu} (**2**) (56.3 mg, 142.0 µmol), TlPF$_6$ (145.0 mg, 414.0 µmol) and a magnetic stir bar under inert atmosphere. THF (dry, 25 mL) was added to the mixture and an immediate formation of a colorless precipitate was observed. While stirring, the reaction mixture was heated to reflux and allowed to cool down after 81 h of heating. The off-white precipitate was filtered off with a P4 glass filter frit and the filtrate was transferred into a flask. Layering of the filtrate with hexanes afforded colorless, crystalline material (suitable for XRD) that was separated after 4 h and washed with hexanes. Product [**3**](PF$_6$) was obtained as a colorless crystalline solid in 34% yield (35.3 mg, 43.4 µmol).

Analysis: IR (KBr) ν [cm^{-1}]: 3434*w*, 2999*m*, 2959*m*, 2880*m*, 2047*s* (CO), 1946*s* (CO), 1913*s* (CO), 1601*w*, 1482*m*, 1463*m*, 1395*m*, 1377*m*, 1290*m*, 1183*m*, 1024*w*, 838*s*, 628*m*, 558*m*. **^{1}H NMR** (500 MHz, CD_2Cl_2) δ [ppm]: 7.91 (*t*, $^3J_{HH}$ = 7.83 Hz, 1 H, C$H_{pyr(4)}$); 7.65 (*d*, $^3J_{HH}$ = 7.83 Hz, 2 H, C$H_{pyr(3,5)}$); 3.92 (*dd*-like *t*, $^2J_{HH}$ = 3.08 Hz, 4 H, PCH_2); 1.38 (*t*-like *m*, 36 H, (PC(CH_3)$_3$). **^{13}C{^{1}H} NMR** (125 MHz, CD_2Cl_2) δ [ppm]: 197.3 (*t*, $^2J_{CP}$ = 7.8 Hz, 2 C, 2 *trans*-*C*O); 196.5 (*t*, $^2J_{CP}$ = 3.6 Hz, 1 C, *C*O); 164.4 (*t*, $^2J_{CP}$ = 2.6 Hz, 2 C, $C_{pyr(2,6)}$); 141.2 (*s*, 1 C, *C*H$_{pyr(4)}$); 123.3 (*t*, $^3J_{CP}$ = 4.0 Hz, 2 C, *C*H$_{pyr(3,5)}$); 40.9 (*t*, $^2J_{CP}$ = 10.0 Hz, 2 C, P*C*H$_2$); 38.9 (*t*, $^1J_{CP}$ = 9.8 Hz, 4 C, P*C*(CH$_3$)$_3$); 30.3 (*t*, $^2J_{CP}$ = 1.6 Hz, 12 C, PC(*C*H$_3$)$_3$). **^{31}P{^{1}H} NMR** (202 MHz, CD_2Cl_2) δ [ppm]: 67.53 (*s*, 2 P, *P*C(CH$_3$)$_3$); –144.44 (*sep*, $^1J_{PF}$ = 710.8 Hz, 1 P, *P*F$_6$). **^{19}F NMR** (470 MHz, CD_2Cl_2) δ [ppm]: –72.95 (*d*, $^1J_{FP}$ = 710.8 Hz, 6 F, P*F*$_6$). **UHPLC-ESI-MS:** R_t = 3.44 min, [M]$^+$ = calc. for $C_{26}H_{43}NO_3P_2Re$: 666.2 m/z, found: 666.1 m/z and [M–CO]$^+$ = calc. for $C_{25}H_{43}NO_2P_2Re$: 638.2 m/z, found: 638.2 m/z.

3.2 *mer*–[Re(^{Pyr}PNP^{tBu})(CO)$_3$]$^+$, [3](BF$_4$)

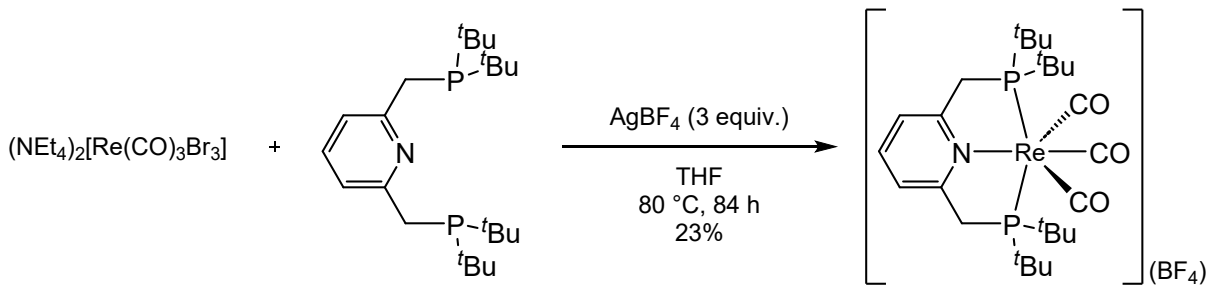

(NEt$_4$)$_2$[**1**] **2** [**3**](BF$_4$)

Synthesis: The synthesis of [**3**](BF$_4$) followed an analogous procedure as in the synthesis of [3](PF$_6$) (3.1). (NEt$_4$)$_2$[**1**] (25.0 mg, 32.3 µmol), ^{Pyr}PNP^{tBu} (**2**) (14.0 mg, 36.0 µmol) and AgBF$_4$ (18.0 mg, 92.8 µmol) were mixed in a round-bottom flask and dry THF (25 mL) was added under inert atmosphere.

The stirred mixture was heated to reflux for 84 h and subsequently the grey suspension was filtered (P4). The solvent of the slightly pale yellowish filtrate was removed *in vacuo* and pale yellowish crystalline material was obtained and characterized to be [**3**](BF_4) in a yield of 23% (6.9 mg, 9.16 µmol).

Analysis: c.f. 3.2 for [**3**](PF_6), IR bands of BF_4^- (KBr) ν [cm^{-1}]: 1463*m*, 1374*m*, 1061*s*.

3.3 *mer*–[Tc(^{Pyr}PNP^{tBu})(CO)$_3$]$^+$, [5](PF$_6$)

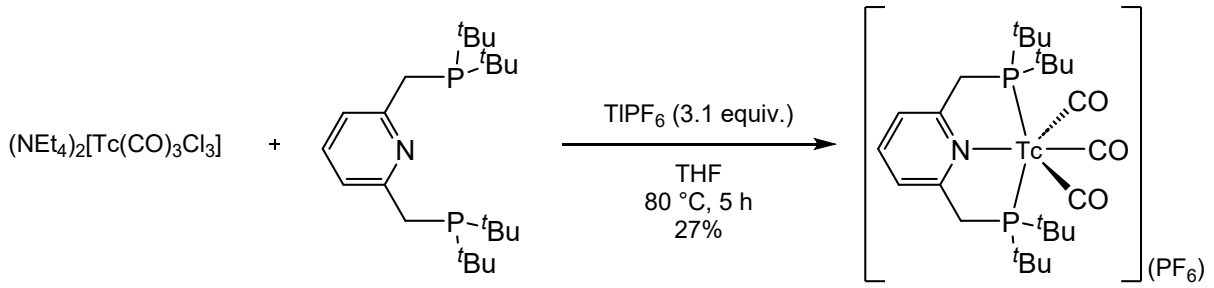

(NEt$_4$)$_2$[**4**] **2** [**5**](PF$_6$)

Synthesis: A round-bottom flask was charged with (NEt$_4$)$_2$[**4**] (23.3 mg, 42.5 µmol), ^{Pyr}PNP^{tBu} (**2**) (25.0 mg, 63.2 µmol, 1.5 equiv.), $TlPF_6$ (45.0 mg, 128.6 µmol, 3 equiv.) and a magnetic stir bar under inert atmosphere. THF (dry, 15 mL) was added to the mixture and an immediate formation of a colorless precipitate was observed. While stirring, the reaction mixture was heated to reflux for 5 h and subsequently allowed to cool down. The off-white precipitate was filtered off with a P4 glass filter frit and the filtrate was transferred into a vial. Layering of the filtrate with hexanes afforded slightly yellowish colored crystals of [**5**](PF_6) in 27% yield (8.27 mg, 11.5 µmol).

Analysis: IR (KBr) ν [cm^{-1}]: 3434*w*, 2973*m*, 2878*w*, 2053*w* (CO), 1960*s* (CO), 1923*s* (CO), 1624*w*, 1480*m*, 1462*m*, 1396*w*, 1289*w*, 1182*w*, 1023*m*, 895*m*, 839*s*, 630*w*, 558*m*. **^{1}H NMR** (400 MHz, CD_2Cl_2) δ [ppm]: 7.86 (*t*, $^3J_{HH}$ = 7.96 Hz, 1 H, C$H_{pyr(4)}$); 7.57 (*d*, $^3J_{HH}$ = 7.84 Hz, 2 H, C$H_{pyr(3,5)}$); 3.71 (*t*-like *m*, $^2J_{HH}$ = 2.50 Hz, 4 H, PCH_2); 1.37 (*t*-like *m*, 36 H, (PC(CH_3)$_3$). **^{13}C{^{1}H} NMR** (126 MHz, CD_2Cl_2) δ [ppm]: 163.0 (*t*, $^2J_{CP}$ = 2.7 Hz, 2 C, $C_{pyr(2,6)}$); 140.9 (*s*, 1 C, $CH_{pyr(4)}$); 123.5 (*t*, $^3J_{CP}$ = 4.0 Hz, 2 C, $CH_{pyr(3,5)}$); 39.0 (*t*, $^2J_{CP}$ = 7.9 Hz, 2 C, PCH_2); 38.4 (*t*, $^1J_{CP}$ = 7.7 Hz, 4 C, PC(CH$_3$)$_3$); 30.4 (*t*-like s, 12 C, PC(CH_3)$_3$); ^{13}C signals of CO ligands not observed (c.f. section 3.8). **^{31}P{^{1}H} NMR** (202 MHz, CD_2Cl_2) δ [ppm]: 90.78 (br *s*, $\Delta_{1/2}$ = 4.4 kHz, 2 P, *P*C(CH$_3$)$_3$); –142.71 (*sep*, $^1J_{PF}$ = 711.68 Hz, 1 P, *P*F$_6$). **^{19}F NMR** (471 MHz, CD_2Cl_2) δ [ppm]: –73.08 (*d*, $^1J_{FP}$ = 710.6 Hz, 6 F, P*F*$_6$). **^{99}Tc NMR** (90.1 MHz, C_6D_6) δ [ppm]: -1574 ($\Delta_{1/2}$ = 2.2 kHz). **^{99}Tc analysis** calc. for $C_{26}H_{43}F_6NO_3P_3Tc$ (·Et_4NPF_6) (%): 9.90; found: 8.89.

3.4 *mer*–[^{99m}Tc(^{Pyr}PNP^{tBu})(CO)$_3$], [7]$^+$

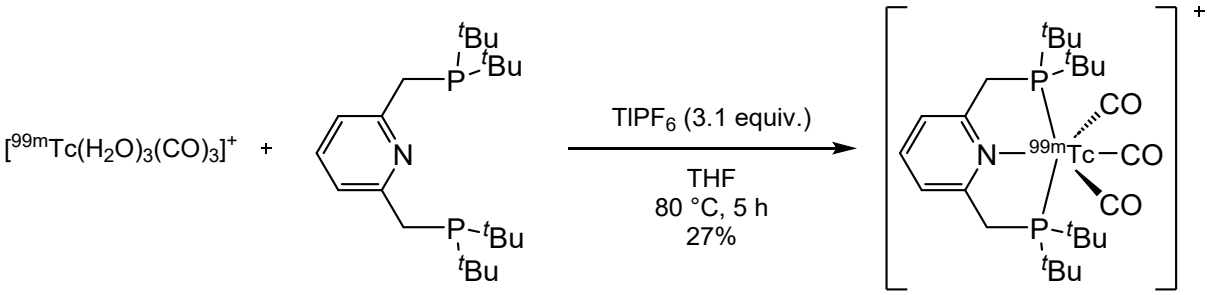

[**6**]$^+$ **2** [**7**]$^+$

Synthesis: Method a: A microwave vial was charged with 1.0 mL of an aqueous solution containing freshly prepared [^{99m}Tc(H_2O)$_3$(CO)$_3$]$^+$ ([**6**]$^+$). The vial was sealed and flushed with N_2 for 15 min and in a separate vial ^{Pyr}PNP^{tBu} (**2**) (10.1 mg, 25.5 µmol) was dissolved in 1 mL of degassed EtOH. The EtOH solution of 2 was added to the sealed vial with a syringe and subsequently the vial was placed in the microwave for 30 min at 100 °C. Complex [**7**]$^+$ was obtained with 92% RCP and purification with radio-HPLC delivered [**7**]$^+$ in 97% RCP. (RCY: 95%).

Method b: Alternatively, [**7**]$^+$ may also be synthesized in a 1-pot reaction with eluted [^{99m}TcO$_4$]$^-$ in presence of the *isolink kit* chemicals and ^{Pyr}PNP^{tBu} (**2**) in a H_2O/EtOH (1:1, degassed) solution, yielding equivalent results after 30 min at 100 °C in the microwave.

Analysis: Radio-HPLC: R_t = 25.53 min, RCP: 97.1%.

3.5 *fac*–[Re(κ^2–terpy)(CO)$_3$(PO_2F_2)], [9]

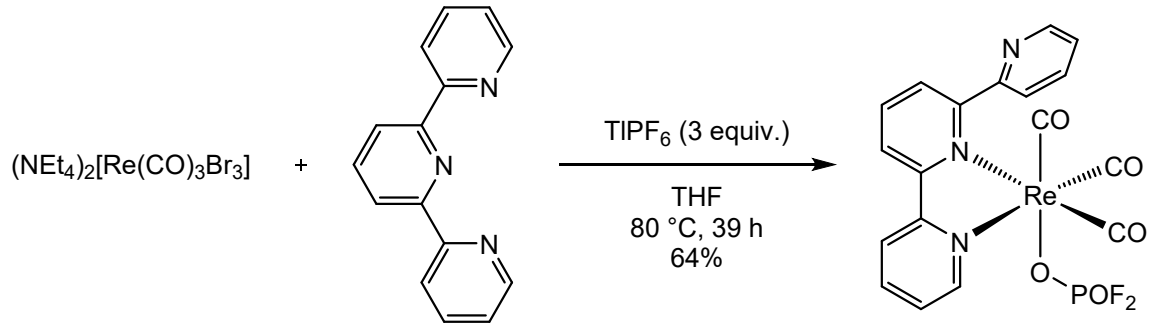

(NEt$_4$)$_2$[**1**] **8** [**9**]

Synthesis: A round-bottom flask was charged with (NEt$_4$)$_2$[**1**] (50.4 mg, 65.4 µmol), terpy (**8**) (16.3 mg, 69.9 µmol, 1.1 equiv.), $TlPF_6$ (67.8 mg, 194.1 µmol, 3 equiv.) and a magnetic stir bar under inert atmosphere. THF (dry, 10 mL) was added to the mixture and an immediate formation of a colorless precipitate was observed. While stirring, the reaction mixture was heated to reflux for 39 h and subsequently allowed to cool down. The off-white precipitate was filtered off with a P4 glass filter frit and the filtrate was concentrated. Layering of the filtrate with hexanes afforded [**9**] as pale yellowish, crystalline material after washing with hexanes in a yield of 64% (25.4 mg, 42.0 µmol).

Analysis: IR (KBr) ν [cm^{-1}]: 3434*w*, 2924*m*, 2853*m*, 2021*s* (CO), 1916*s* (CO), 1895*s* (CO), 1768*w*, 1719*w*, 1605*w*, 1453*m*, 1313*m* ($PO_2F_2^-$), 1158*m* ($PO_2F_2^-$), 1034*w*, 842*s* ($PO_2F_2^-$), 775*m*, 647*w*, 558*w*, 498*w* ($PO_2F_2^-$). **^{1}H NMR** (400 MHz, THF-d_8) δ [ppm]: 9.14 (*d*, $^3J_{HH}$ = 5.2 Hz, 1 H, C$H_{terpy\text{-}1}$); 8.77 (*d*, $^3J_{HH}$ = 4.5 Hz, 1 H, C$H_{terpy\text{-}11}$); 8.62 (*t* (2 overlaid *d*), 2 H, C$H_{terpy\text{-}5,4}$); 8.33 (*t*, $^3J_{HH}$ = 7.94 Hz, 1 H, C$H_{terpy\text{-}}$

$_6$); 8.27 (*t*, $^3J_{HH}$ = 7.0 Hz, 1 H, C$H_{terpy\text{-}3}$); 7.95 (*t*, $^3J_{HH}$ = 7.4 Hz, 1 H, C$H_{terpy\text{-}9}$); 7.88 (*t* (2 overlaid *d*), 2 H, C$H_{terpy\text{-}8,7}$); 7.71 (*t*, $^3J_{HH}$ = 6.4 Hz, 1 H, C$H_{terpy\text{-}2}$); 7.52 (*t*, $^3J_{HH}$ = 6.2 Hz, 1 H, C$H_{terpy\text{-}10}$). **^{31}P{^{1}H} NMR** (162 MHz, THF-d_8) δ [ppm]: –16.19 (*t*, $^1J_{FP}$ = 961.7 Hz, 1 P, PO_2F_2). **^{19}F{^{1}H} NMR** (376 MHz, THF-d_8) δ [ppm]: –73.66 (*d*, $^1J_{FP}$ = 710.30 Hz, 1 F, minimal traces of PF_6 (not visible in ^{31}P{^{1}H})), –84.5 (*d*, $^1J_{FP}$ = 961.3 Hz, 2 F, PO_2F_2). **UHPLC-ESI-MS:** R_t = 2.26 min, [M-($PO_2F_2^-$)]$^+$ = calc. for $C_{18}H_{11}N_3O_3Re$: 504.0 m/z, found: 504.0 m/z and [M–($PO_2F_2^-$)+MeCN]$^+$ = calc. for $C_{25}H_{43}NO_2P_2Re$: 545.1 m/z, found: 545.0 m/z.

3.6 *fac*–[Re(κ^2–terpy)(CO)$_3$Br], [10]

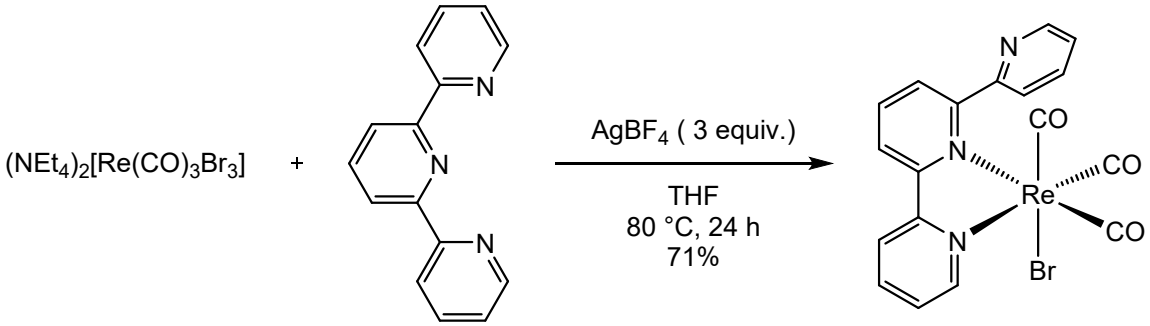

(NEt$_4$)$_2$[**1**] **8** [**10**]

Synthesis: A round-bottom flask was charged with (NEt$_4$)$_2$[**1**] (47.7 mg, 61.9 µmol), terpy (**8**) (15.8 mg, 67.8 µmol, 1.1 equiv.), $AgBF_4$ (36.0 mg, 184.9 µmol, 3 equiv.) and a magnetic stir bar under inert atmosphere. THF (dry, 12 mL) was added to the mixture and an immediate formation of a yellowish suspension was observed. While stirring, the reaction mixture was heated to reflux for 24 h and subsequently allowed to cool down. The greyish precipitate was filtered off with a P4 glass filter frit and the solvent of the greenish-yellowish filtrate was evaporated *in vacuo*. The residue was washed with H_2O (3x5 mL) and subsequently redissolved in minimal THF. Layering of the solution with hexanes afforded [**10**] as yellow, crystalline material after washing with hexanes in a yield of 71% (25.7 mg, 44.1 µmol).

Analysis: Complex [**10**] has already been obtained via a different route published by Abel, *et al.*[14] and the obtained data is in agreement.

3.7 *fac*–[Tc(κ^2–terpy)(CO)$_3$Cl], [11]

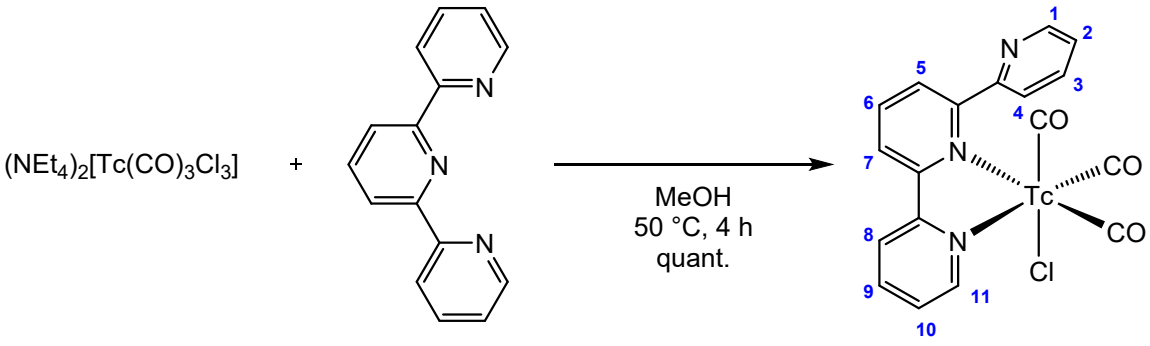

(NEt$_4$)$_2$[**4**] **8** [**11**]

Synthesis: (NEt$_4$)$_2$[**4**] (39.9 mg, 72.6 µmol) was dissolved in 5 mL of MeOH and stirred in a round-bottom flask. Terpy (**8**) (17.3 mg, 74.0 µmol, 1 equiv.) was dissolved in 2 mL of MeOH and added to

stirred solution. The yellow solution was heated to 50 °C for 4 h while the color changed to pale green. After cooling, the solvent was evaporated under a stream N_2 and the remaining solid was washed by stirring in water. The solution was decanted and the residue was dried. The product was extracted with CH_2Cl_2 and subsequently overlaid with hexanes. Crystallization yielded olive-green crystals of [**11**] in quantitative yield.

Analysis: IR (KBr) ν [cm^{-1}]: 3446*w*, 2989*w*, 2026*s* (CO), 1914*s* (CO), 1887*s* (CO), 1460*m*, 1402*w*, 1308*w*, 1184*w*, 1033*w*, 1005*w*, 798*w*, 667*w*, 636*w*, 502*w*. **^{1}H NMR** (400 MHz, CD_2Cl_2, T = 298 K) δ [ppm]: 8.99 (br *s*, 1 H, C$H_{terpy-1}$); 8.81 (br *s*, 1 H, C$H_{terpy-11}$); 8.27 (br *s*, 2 H, C$H_{terpy-4,5}$); 8.16 (*t*, $^3J_{HH}$ = 7.76 Hz, 1 H, C$H_{terpy-6}$); 8.08 (br *s*, 1 H, C$H_{terpy-3}$); 7.93 (br *s*, 2 H, C$H_{terpy-8,9}$); 7.78 (br *s*, 1 H, C$H_{terpy-7}$); 7.53 (br *s*, 2 H, C$H_{terpy2,10}$). **^{1}H NMR** (400 MHz, CD_2Cl_2, T = 235 K) δ [ppm]: 8.96 (*d*, $^3J_{HH}$ = 4.65 Hz, 1 H, C$H_{terpy-1}$); 8.79 (*d*, $^3J_{HH}$ = 4.40 Hz, 1 H, C$H_{terpy-11}$); 8.30 (*d*, $^3J_{HH}$ = 7.90 Hz, 1 H, C$H_{terpy-5}$); 8.27 (*d*, $^3J_{HH}$ = 8.25 Hz, 1 H, C$H_{terpy-4}$); 8.16 (*t*, $^3J_{HH}$ = 7.75 Hz, 1 H, C$H_{terpy-6}$); 8.08 (*t*, $^3J_{HH}$ = 7.63 Hz, 1 H, C$H_{terpy-3}$); 7.94 (*t*, $^3J_{HH}$ = 6.98 Hz, 1 H, C$H_{terpy-9}$); 7.82 (*d*, $^3J_{HH}$ = 7.45 Hz, 1 H, C$H_{terpy-8}$); 7.75 (*d*, $^3J_{HH}$ = 7.45 Hz, 1 H, C$H_{terpy-7}$); 7.53 (*p* (2 overlaid *t*), 2 H, C$H_{terpy-2,10}$). **^{13}C{^{1}H} NMR** (125 MHz, CD_2Cl_2) δ [ppm]: 152.8 (*s*, 1 C, *C*H$_{terpy}$); 149.7 (*s*, 1 C, *C*H$_{terpy}$); 139.3 (*s*, 1 C, *C*H$_{terpy}$); 138.9 (*s*, 1 C, *C*H$_{terpy}$); 136.9 (*s*, 1 C, *C*H$_{terpy}$); 127.3 (*s*, 1 C, *C*H$_{terpy}$); 126.0 (*s*, 1 C, *C*H$_{terpy}$); 125.4 (*s*, 1 C, *C*H$_{terpy}$); 124.8 (*s*, 1 C, *C*H$_{terpy}$); 123.6 (*s*, 1 C, *C*H$_{terpy}$); 122.2 (*s*, 1 C, *C*H$_{terpy}$). **^{99}Tc NMR** (90.1 MHz, CD_2Cl_2) δ [ppm]: -1002 ($\Delta_{1/2}$ = 380 Hz). **^{99}Tc analysis** calc. for $C_{18}H_{11}ClN_3O_3Tc$ (%): 21.90; found: 20.61.

3.8 Fluxional behaviour of *fac*–[Tc(κ^2–terpy)(CO)$_3$Cl], [11]

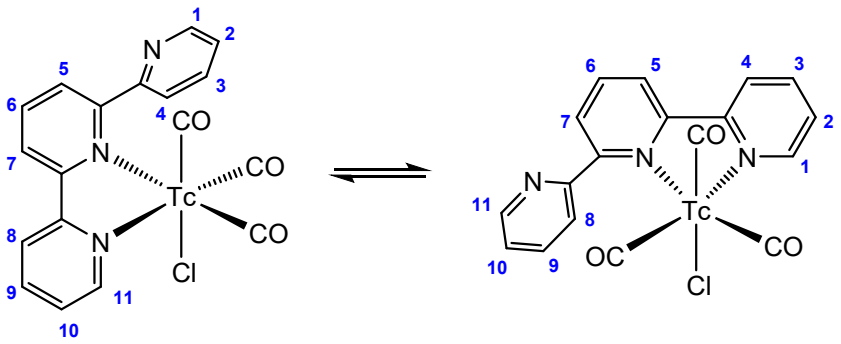

[**11**]

Scheme S1: Fluxional behaviour of the (κ^2–terpy) ligand in complex [**11**]. The scheme shows both interconverting structures with NMR numbering (3.7).

4 Spectra

4.1 *mer*–[Re(^{Pyr}PNP^{tBu})(CO)$_3$]$^+$, [3](PF$_6$)

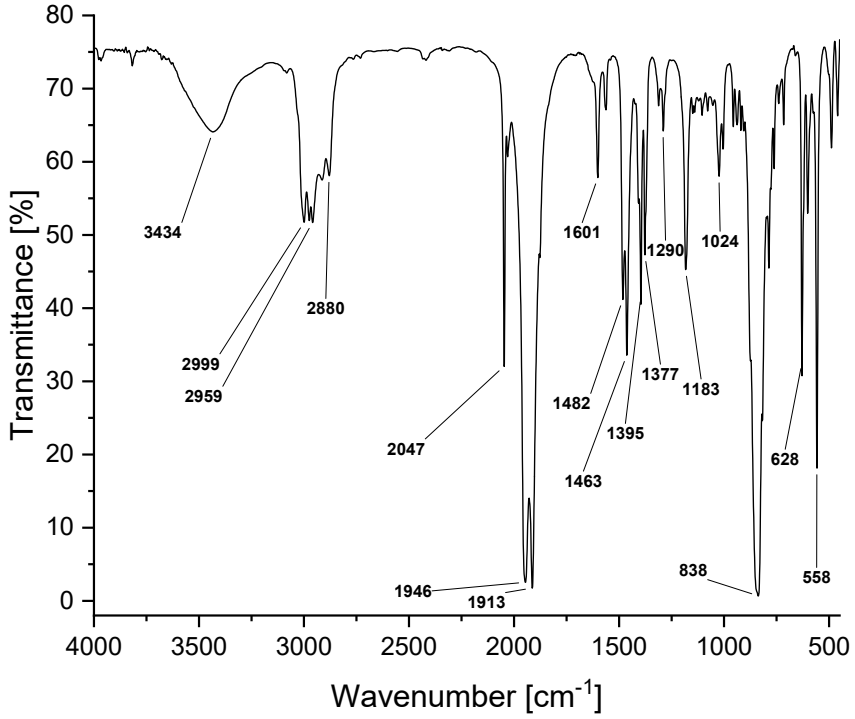

Figure S 1: IR spectrum (KBr) of *mer*–[Re(^{Pyr}PNP^{tBu})(CO)$_3$]$^+$, [**3**](PF$_6$).

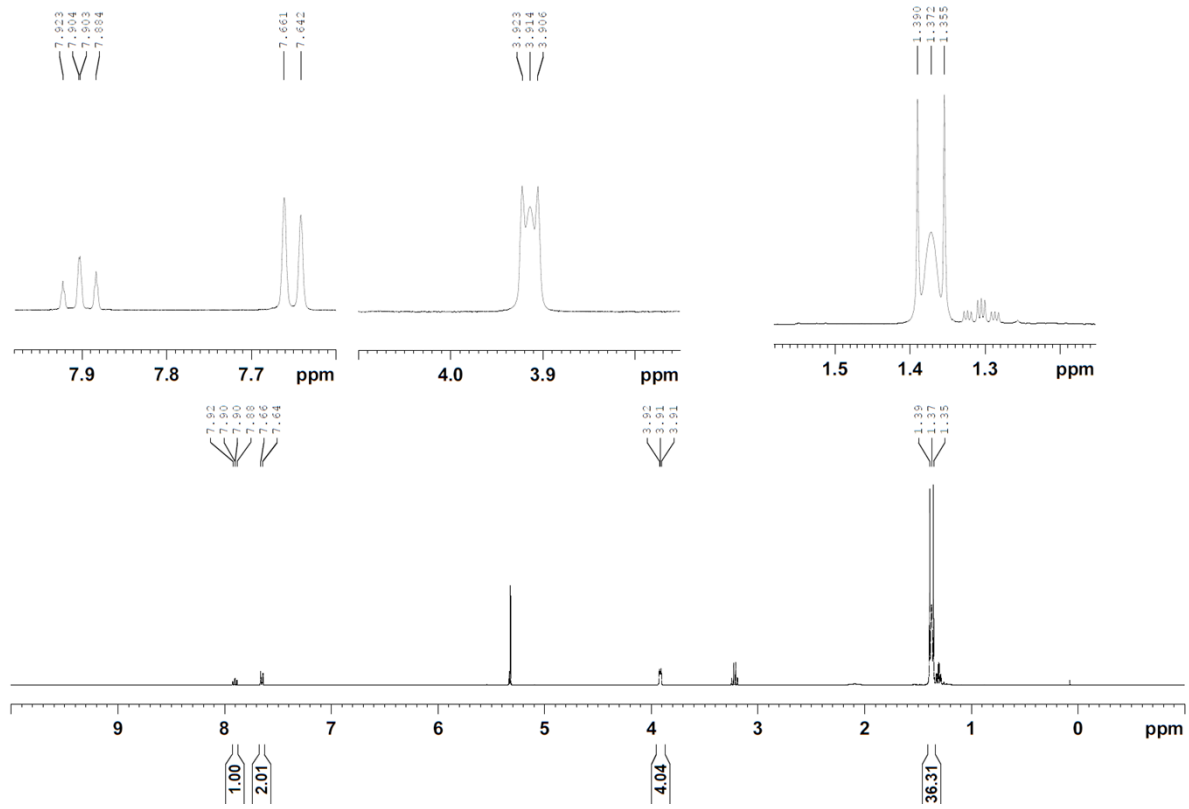

Figure S 2: ^{1}H NMR spectrum of *mer*–[Re(^{Pyr}PNP^{tBu})(CO)$_3$]$^+$, [**3**](PF$_6$) in CD_2Cl_2.

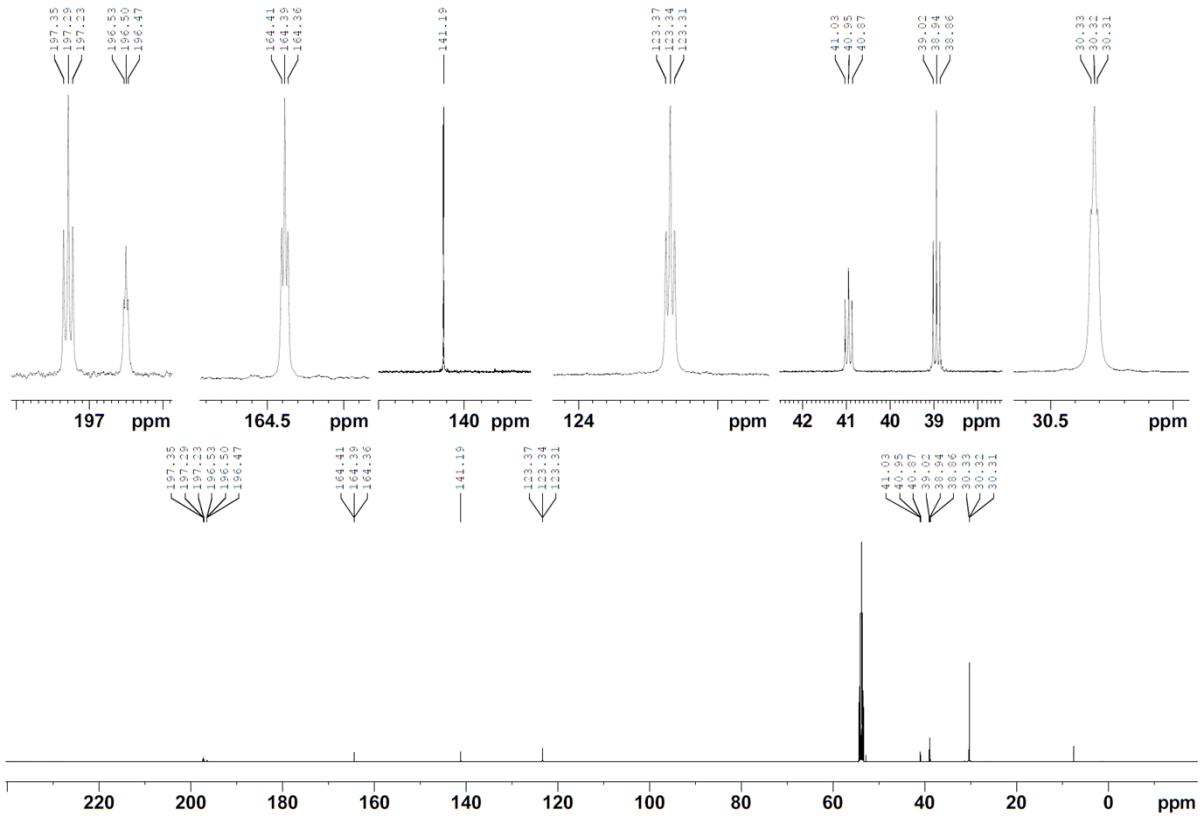

Figure S 3: $^{13}C\{^{1}H\}$ NMR spectrum of *mer*–[Re($^{Pyr}PNP^{tBu}$)$(CO)_3]^+$, [**3**](PF_6) in CD_2Cl_2.

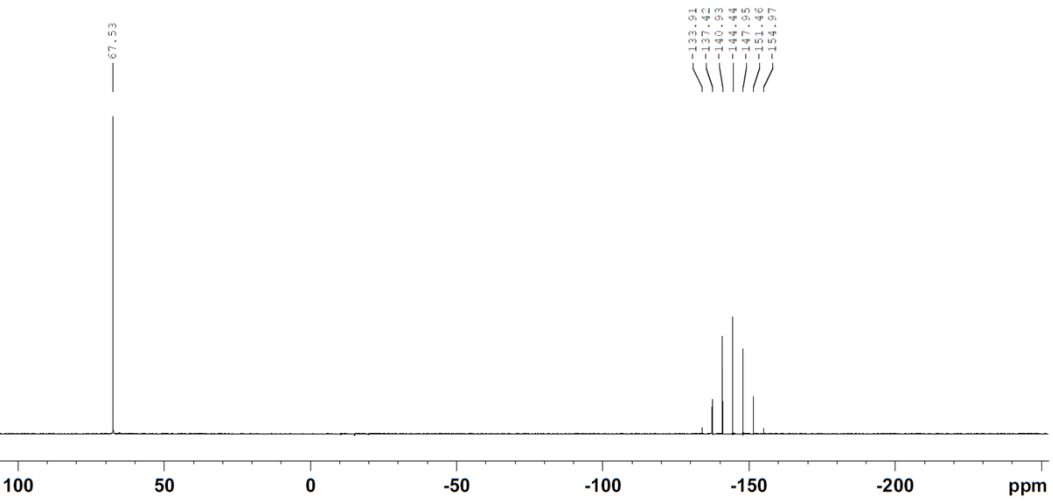

Figure S 4: $^{31}P\{^{1}H\}$ NMR spectrum of *mer*–[Re(^{Pyr}PNP^{tBu})(CO)$_3$]$^+$, [**3**](PF$_6$) in CD_2Cl_2.

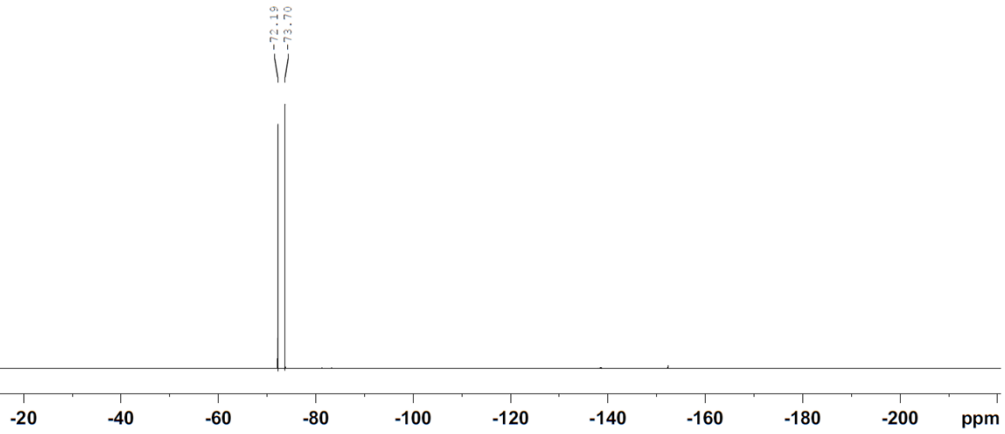

Figure S 5: ^{19}F NMR spectrum of *mer*–[Re(^{Pyr}PNP^{tBu})(CO)$_3$]$^+$, [**3**](PF$_6$) in CD_2Cl_2.

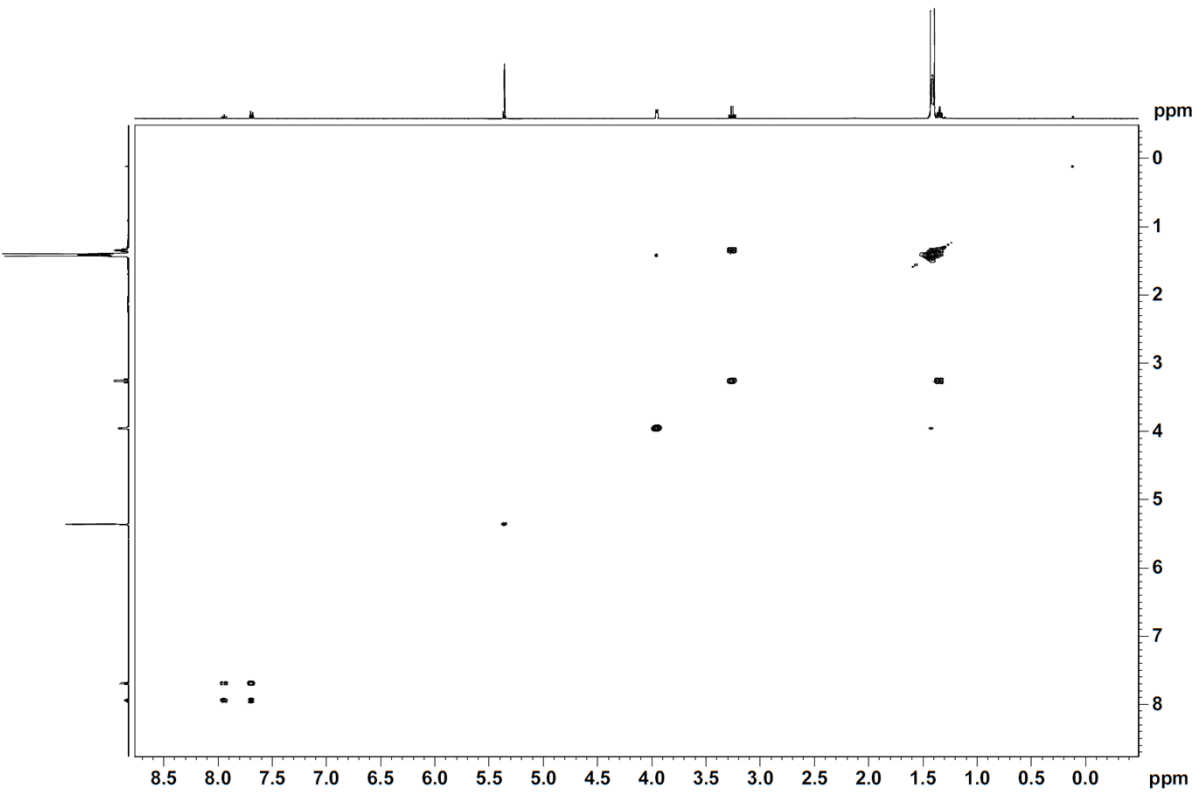

Figure S 6: ^{1}H–^{1}H COSY NMR spectrum of *mer*–[Re($^{Pyr}PNP^{tBu}$)$(CO)_3]^+$, [**3**](PF_6) in CD_2Cl_2.

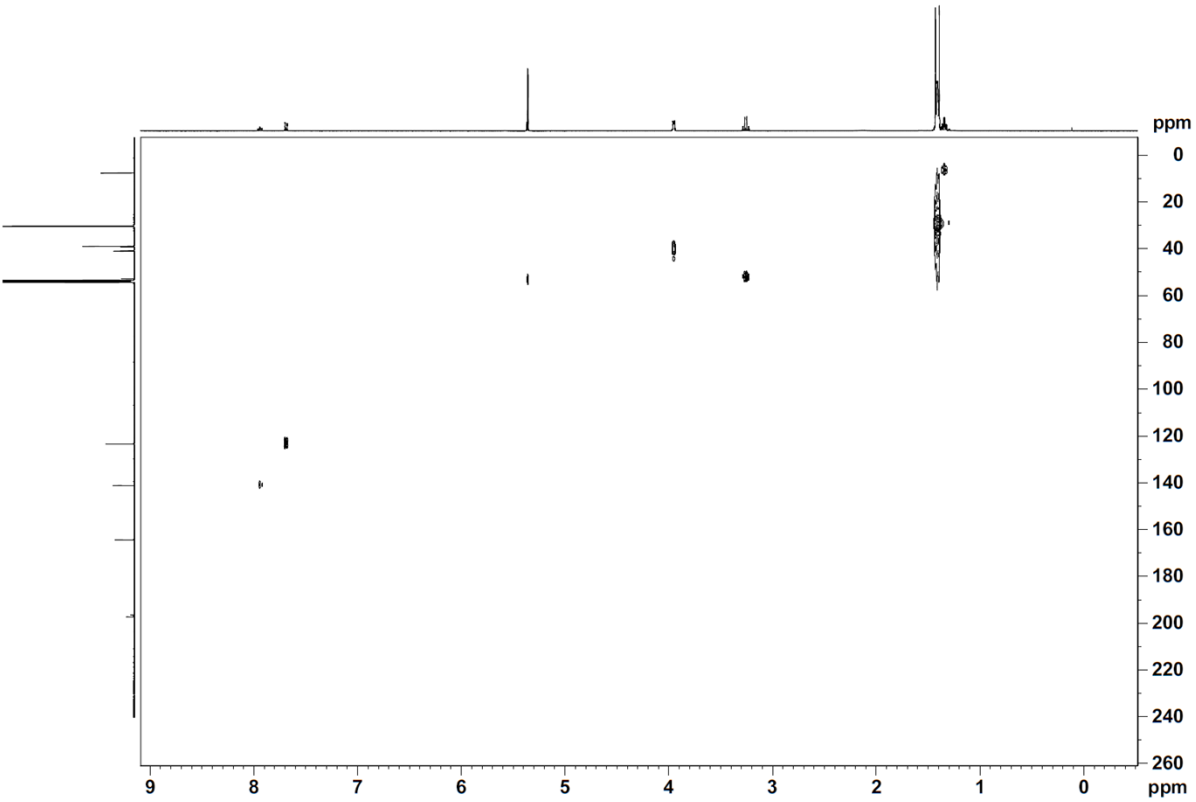

Figure S 7: ^{1}H–^{13}C HSQC NMR spectrum of *mer*–[Re(^{Pyr}PNP^{rBu})(CO)$_3$]$^+$, [**3**](PF$_6$) in CD_2Cl_2.

4.2 *mer*–[Re(^{Pyr}PNP^{tBu})(CO)$_3$]$^+$, [3](BF$_4$)

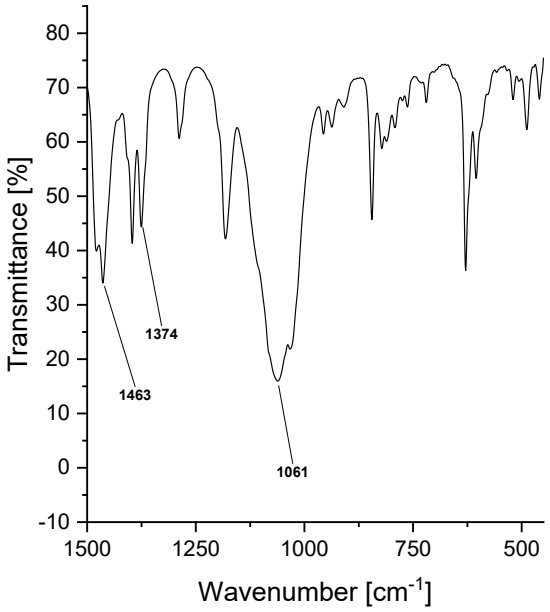

Figure S 8: Excerpt of IR spectrum (KBr) of *mer*–[Re(^{Pyr}PNP^{tBu})(CO)$_3$]$^+$, [**3**](BF$_4$) showing vibrations of BF_4^-.

4.3 *mer*–[Tc(^{Pyr}PNP^{tBu})(CO)$_3$]$^+$, [5](PF$_6$)

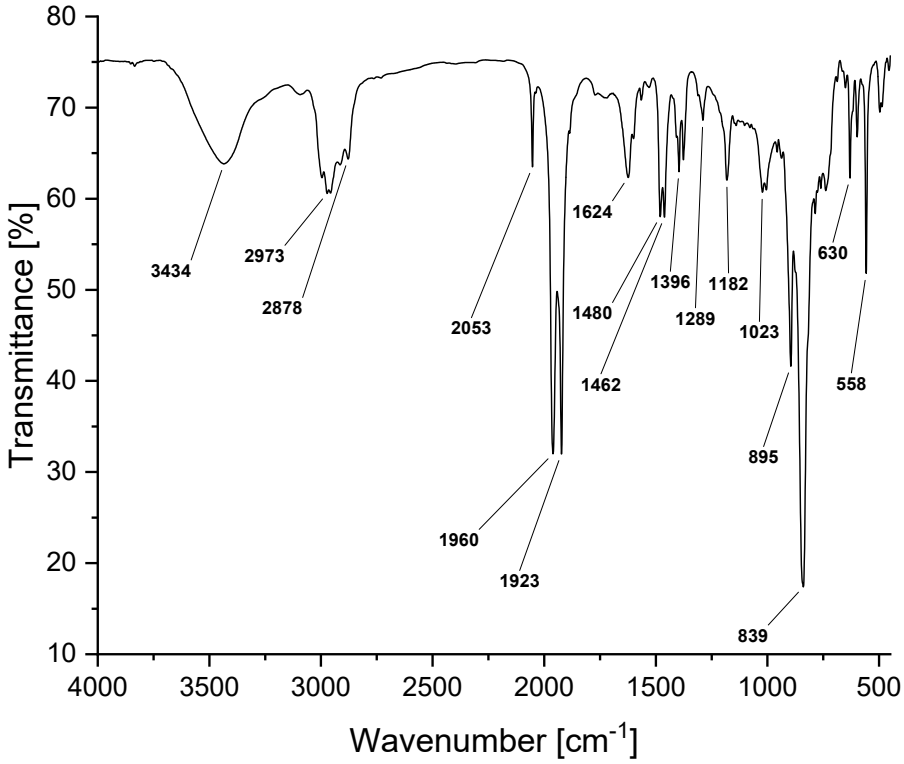

Figure S 9: IR spectrum (KBr) of *mer*–[Tc(^{Pyr}PNP^{tBu})(CO)$_3$]$^+$, [**5**](PF$_6$).

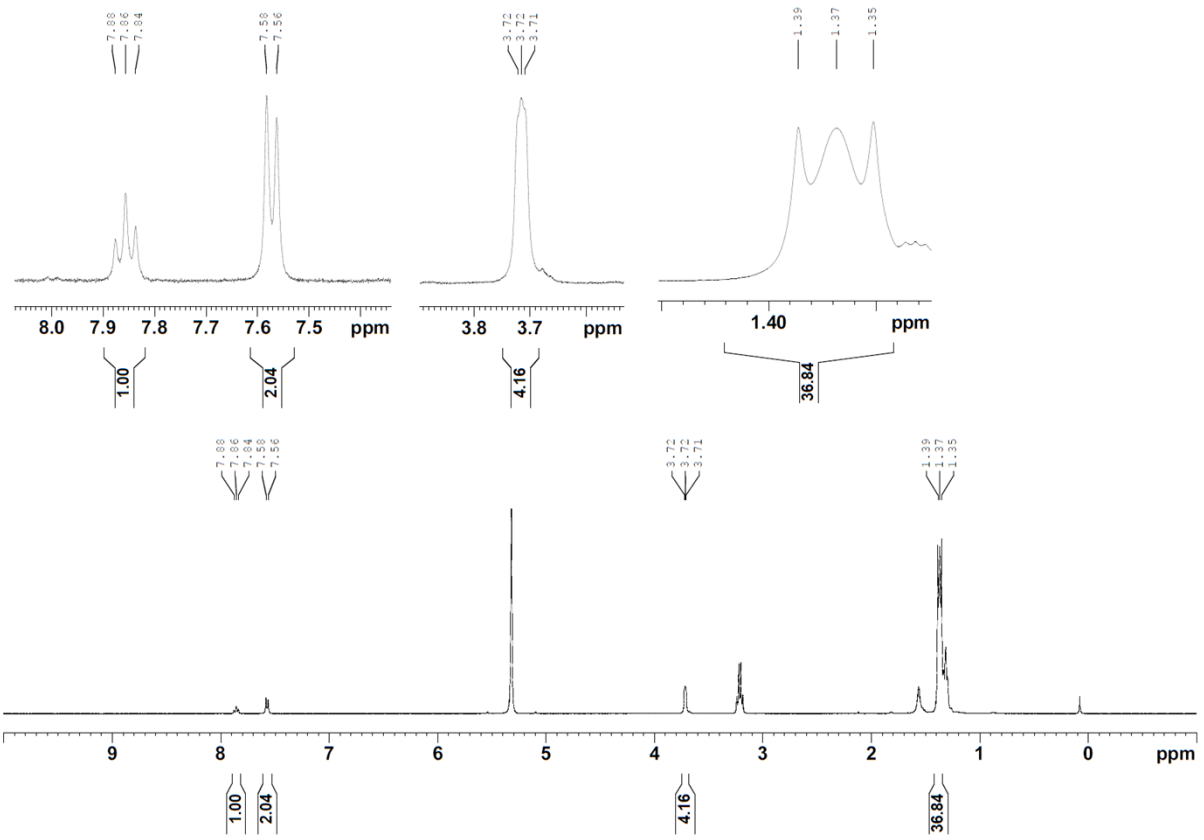

Figure S 10: ^{1}H NMR spectrum of *mer*–[Tc(^{Pyr}PNP^{tBu})(CO)$_3$]$^{+}$, [**5**](PF$_6$) in CD_2Cl_2.

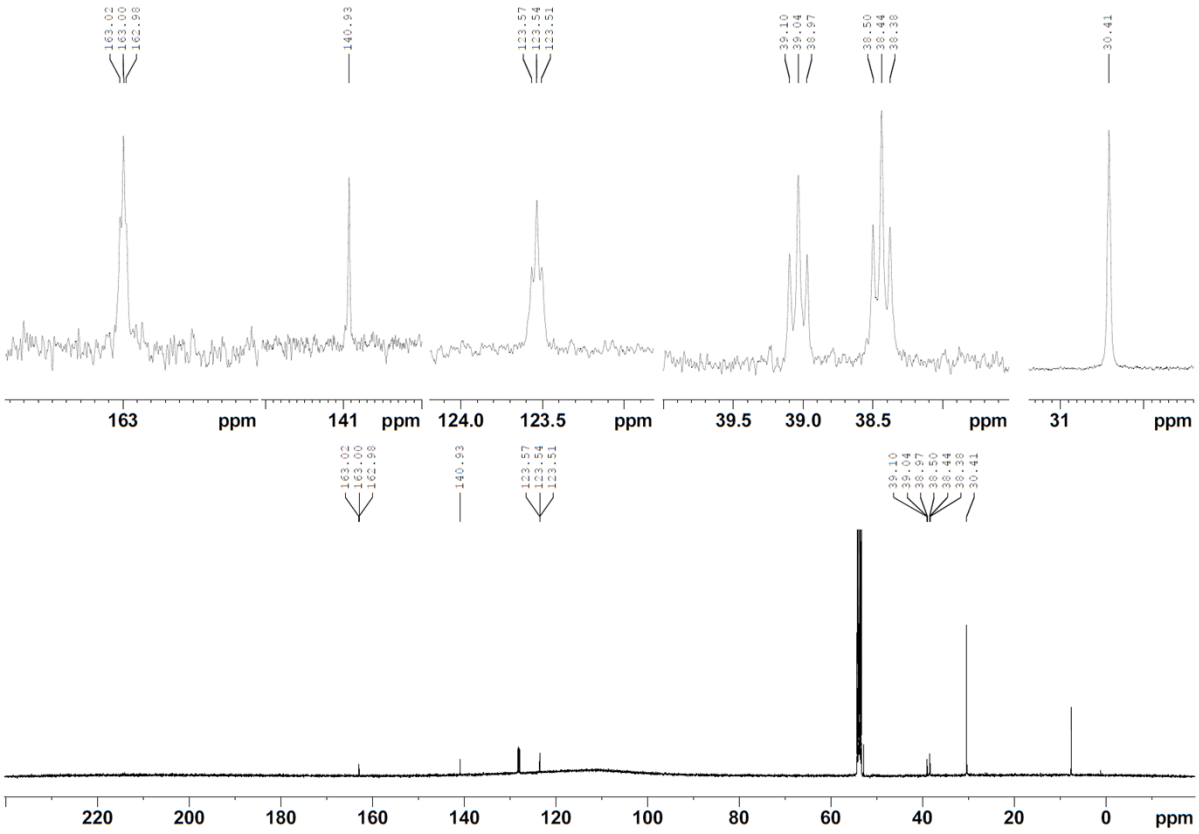

Figure S 11: $^{13}C\{^{1}H\}$ NMR spectrum of *mer*–[Tc(^{Pyr}PNP^{tBu})(CO)$_3$]$^+$, [**5**](PF$_6$) in CD_2Cl_2.

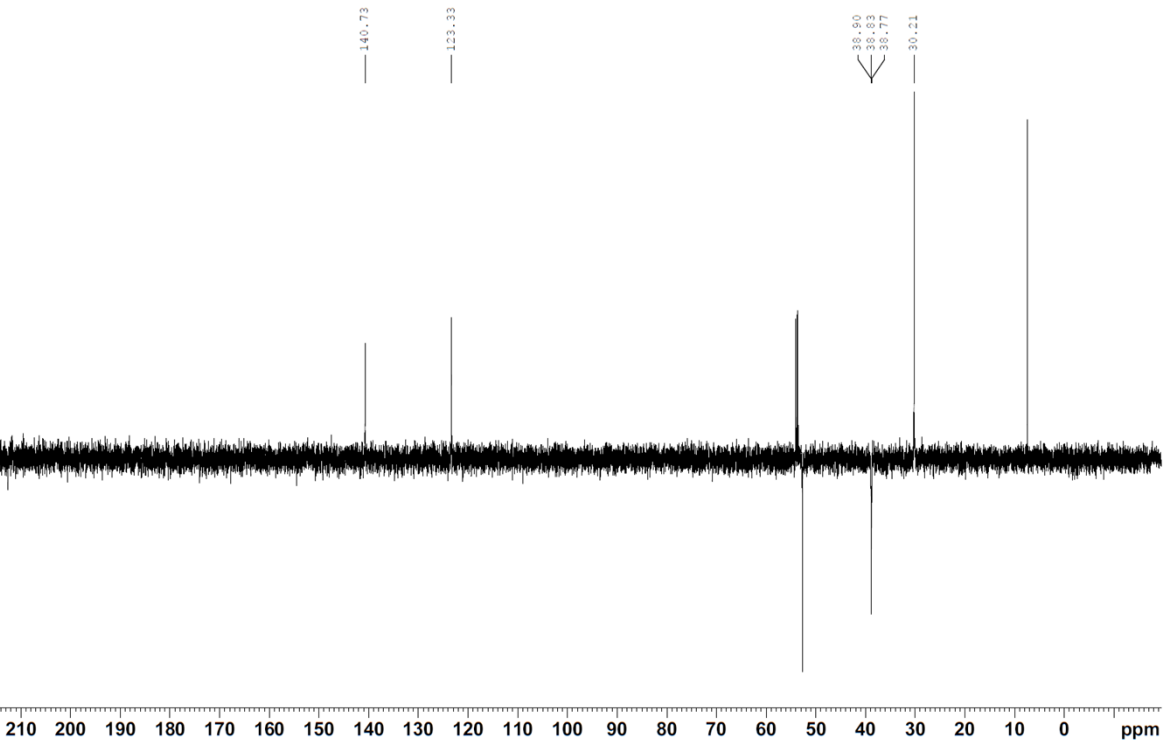

Figure S 12: ^{13}C DEPT-135 NMR spectrum of *mer*–[Tc(^{Pyr}PNP^{tBu})(CO)$_3$]$^+$, [**5**](PF$_6$) in CD_2Cl_2.

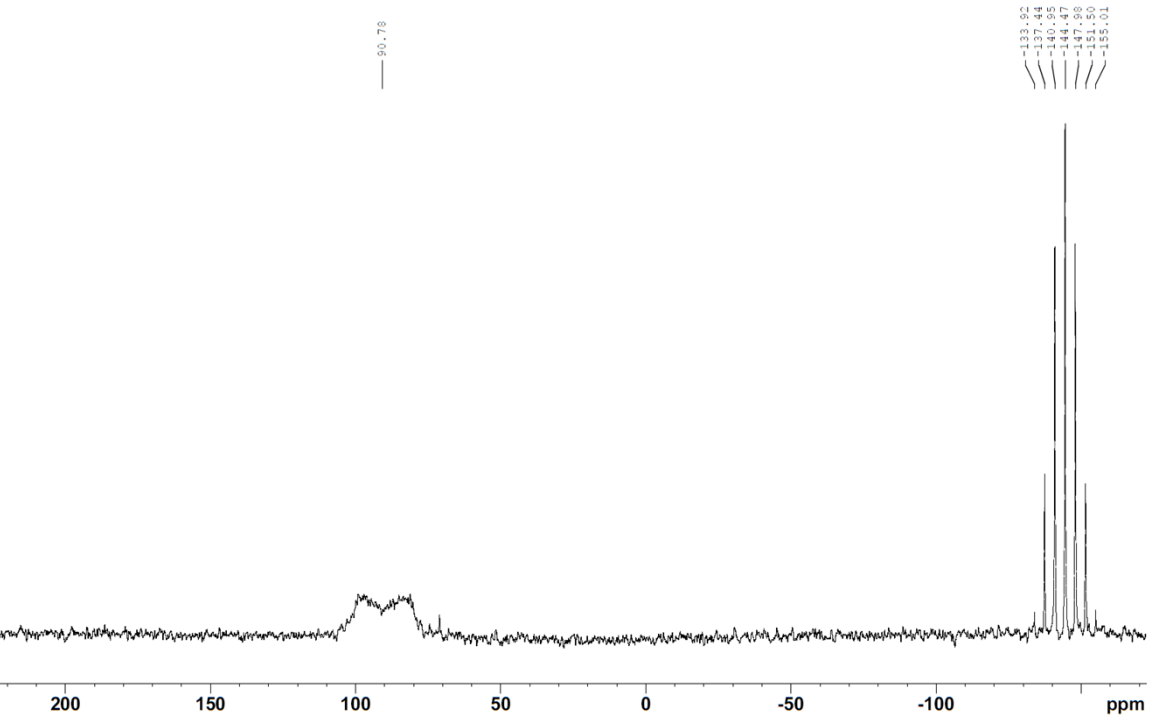

Figure S 13: $^{31}P\{^{1}H\}$ NMR spectrum of *mer*–[Tc(^{Pyr}PNP^{tBu})(CO)$_3$]$^+$, [**5**](PF$_6$) in CD_2Cl_2.

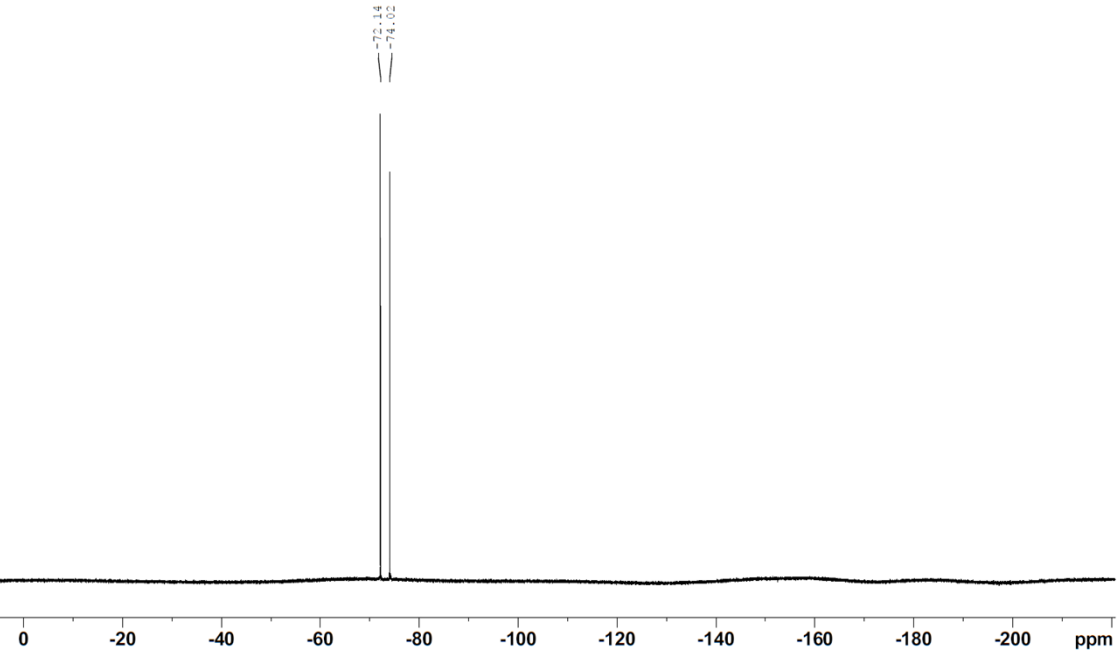

Figure S 14: ^{19}F NMR spectrum of *mer*–[Tc(^{Pyr}PNP^{tBu})(CO)$_3$]$^+$, [**5**](PF$_6$) in CD_2Cl_2.

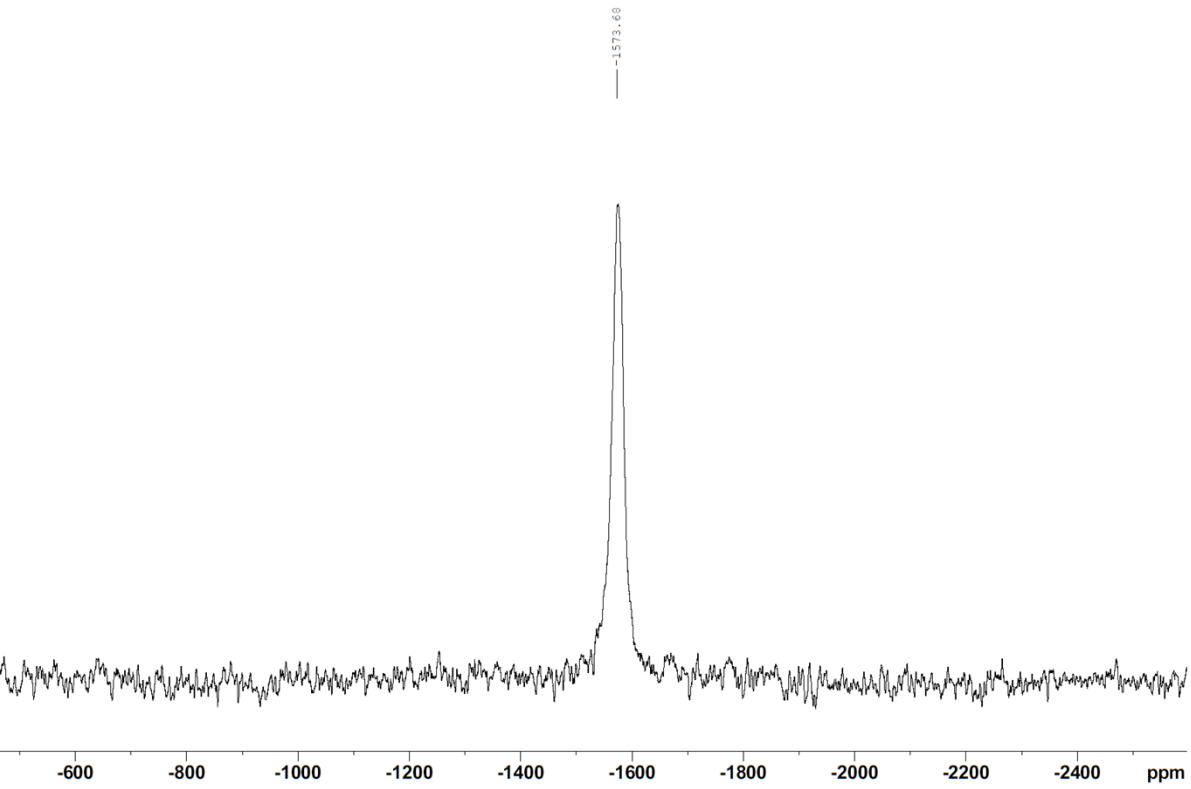

Figure S 15: ^{99}Tc NMR spectrum of *mer*–[Tc(^{Pyr}PNP^{tBu})(CO)$_3$]$^+$, [**5**](PF$_6$) in CD_2Cl_2.

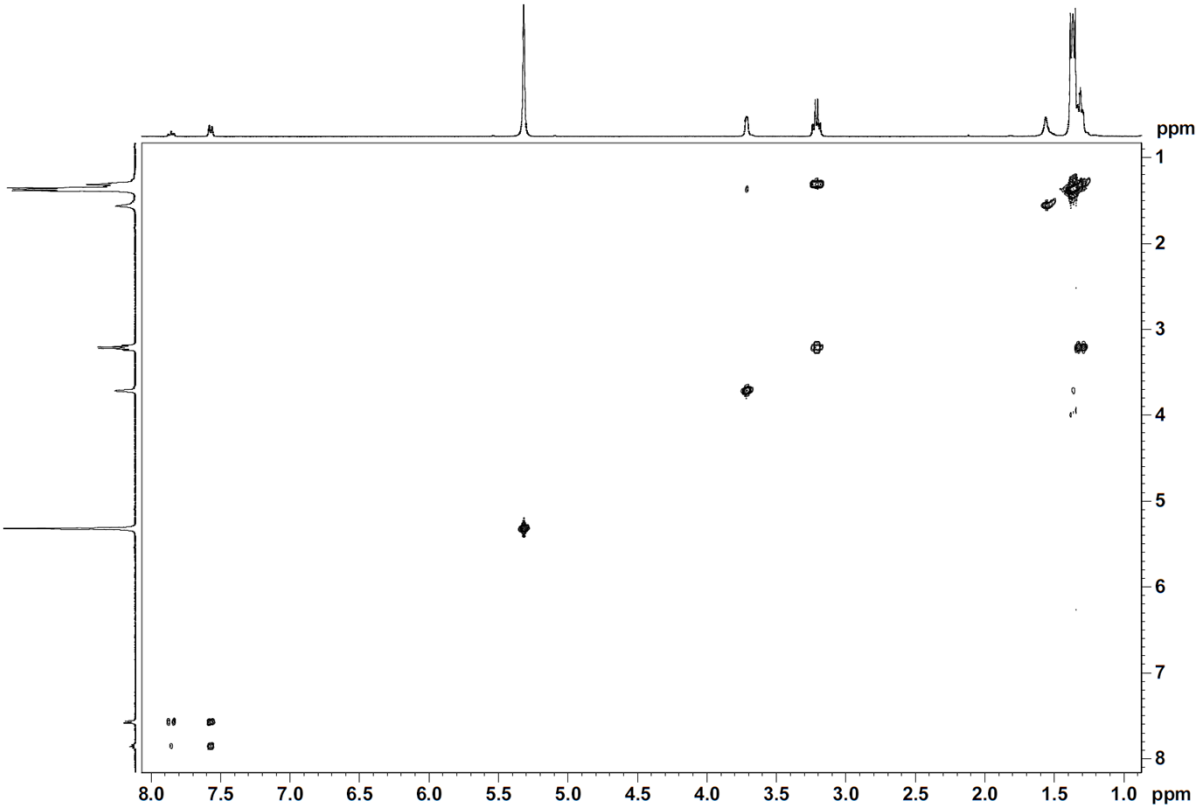

Figure S 16: ^{1}H–^{1}H COSY NMR spectrum of *mer*–[Tc($^{Pyr}PNP^{tBu}$)$(CO)_3]^+$, [**5**](PF_6) in CD_2Cl_2.

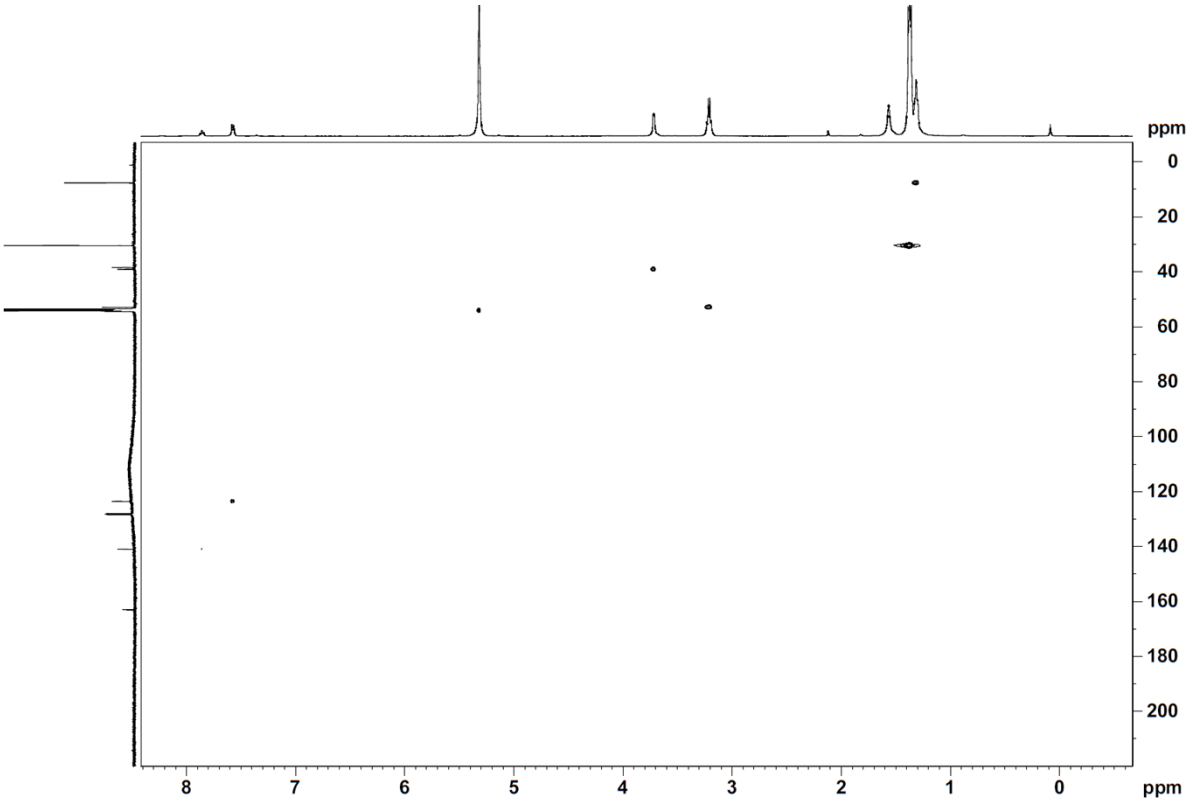

Figure S 17: ^{1}H–^{13}C HSQC NMR spectrum of *mer*–[Tc(^{Pyr}PNP^{tBu})(CO)$_3$]$^+$, [**5**](PF$_6$) in CD_2Cl_2.

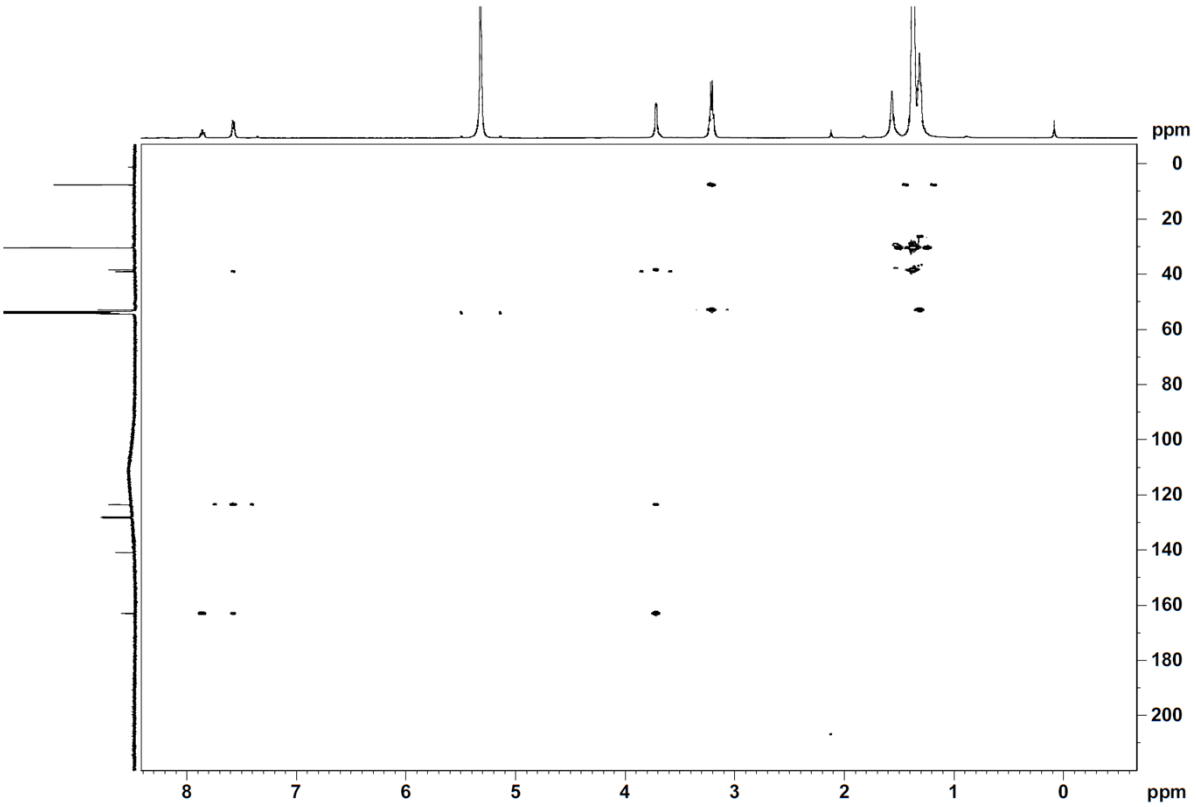

Figure S 18: $^{1}H–^{13}C$ HMBC NMR spectrum of *mer*–[Tc(^{Pyr}PNP^{tBu})(CO)$_3$]$^+$, [**5**](PF$_6$) in CD_2Cl_2.

4.4 *mer*–[^{99m}Tc(^{Pyr}PNP^{tBu})(CO)$_3$], [7]$^+$

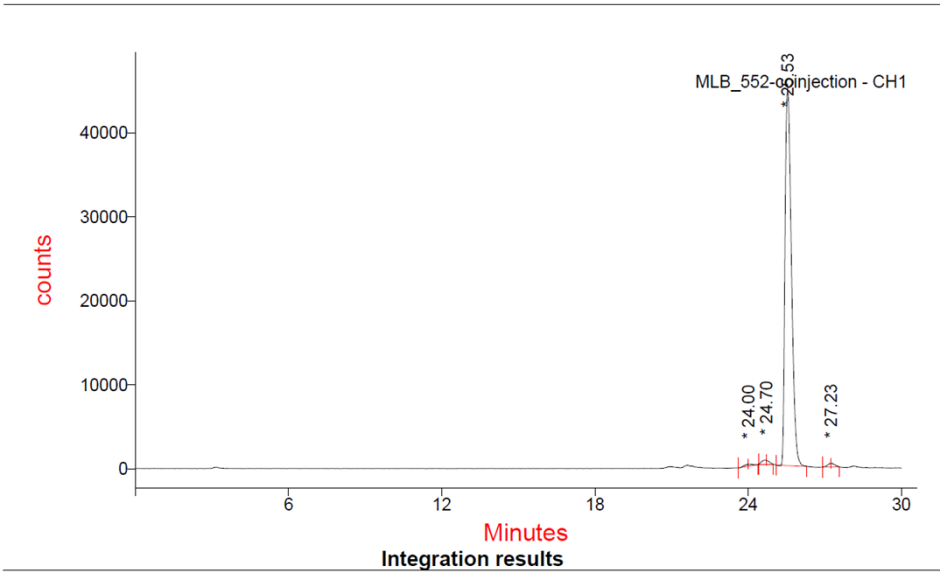

Integration results

#	Rt.	Gross counts	Net counts	% ROI	% All
1	24.00	4640.71	4640.71	0.56	0.48
2	24.70	10493.77	10493.77	1.26	1.08
3	25.53	809645.23	809645.23	97.10	83.51
4	27.23	9026.61	9026.61	1.08	0.93
SUM		**833806.31**	**833806.31**	**100.00**	**86.00**

Figure S 19: γ-trace of *mer*–[^{99m}Tc(^{Pyr}PNP^{tBu})(CO)$_3$]$^+$, [**7**]$^+$.

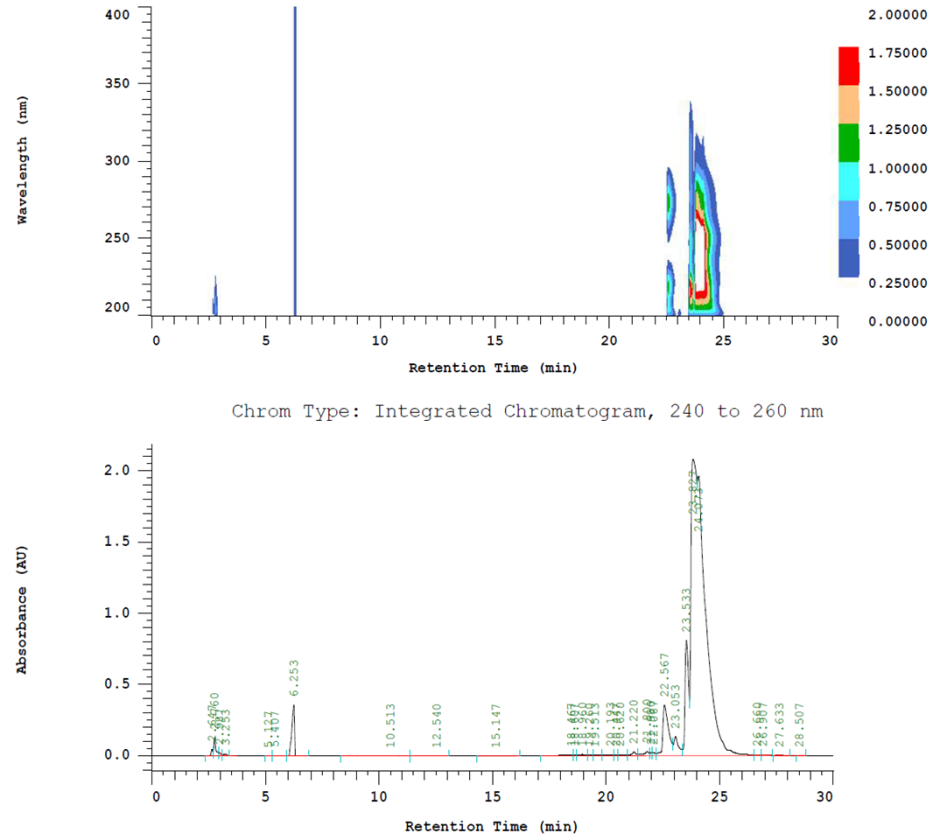

Figure S 20: UV-trace of *mer*–[Tc(^{Pyr}PNP^{tBu})(CO)$_3$]$^+$, [**5**]$^+$.

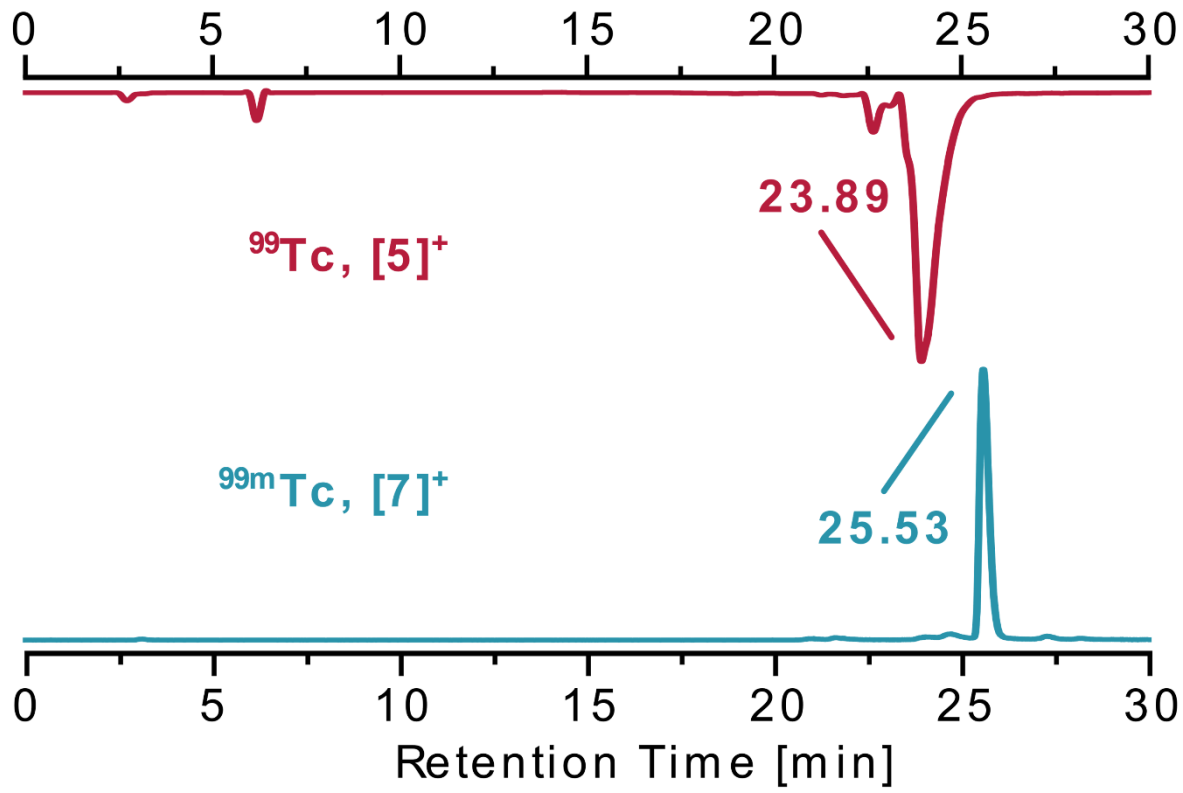

Figure S 21: HPLC traces for the coinjection of *mer*–[Tc(^{Pyr}PNP^{tBu})(CO)$_3$]$^+$, [**5**]$^+$ (top, UV-trace) with *mer*–[^{99m}Tc(^{Pyr}PNP^{tBu})(CO)$_3$]$^+$, [**7**]$^+$ (bottom, γ-trace).

4.5 *fac*–[Re(κ²–terpy)(CO)$_3$(PO$_2$F$_2$)], [9]

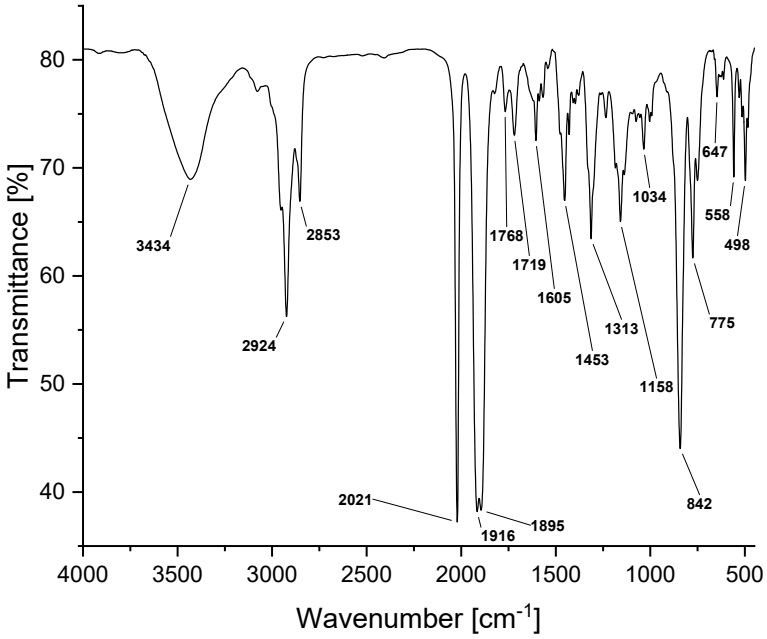

Figure S 22: IR spectrum (KBr) of *fac*–[Re(κ²–terpy)(CO)$_3$(PO$_2$F$_2$)], [**9**].

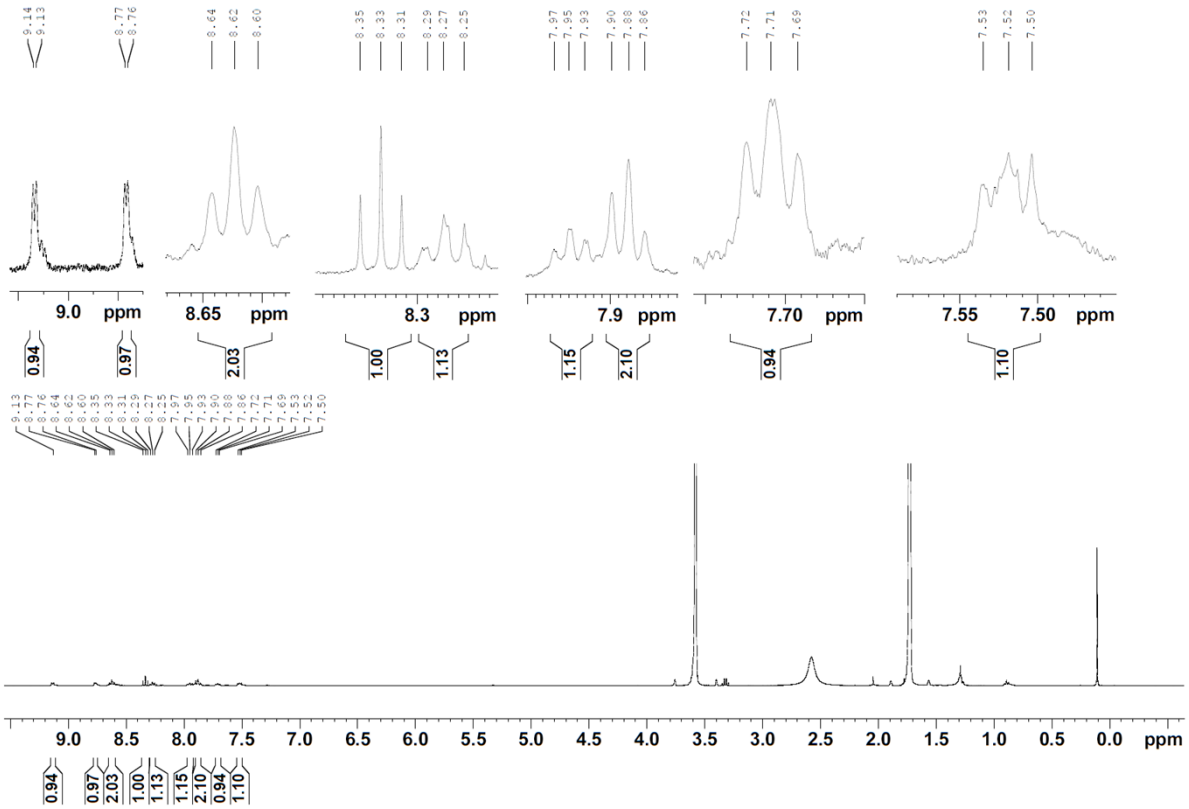

Figure S 23: ^{1}H NMR spectrum of *fac*–[Re(κ^{2}–terpy)(CO)$_3$(PO$_2$F$_2$)], [**9**] in THF-d_8.

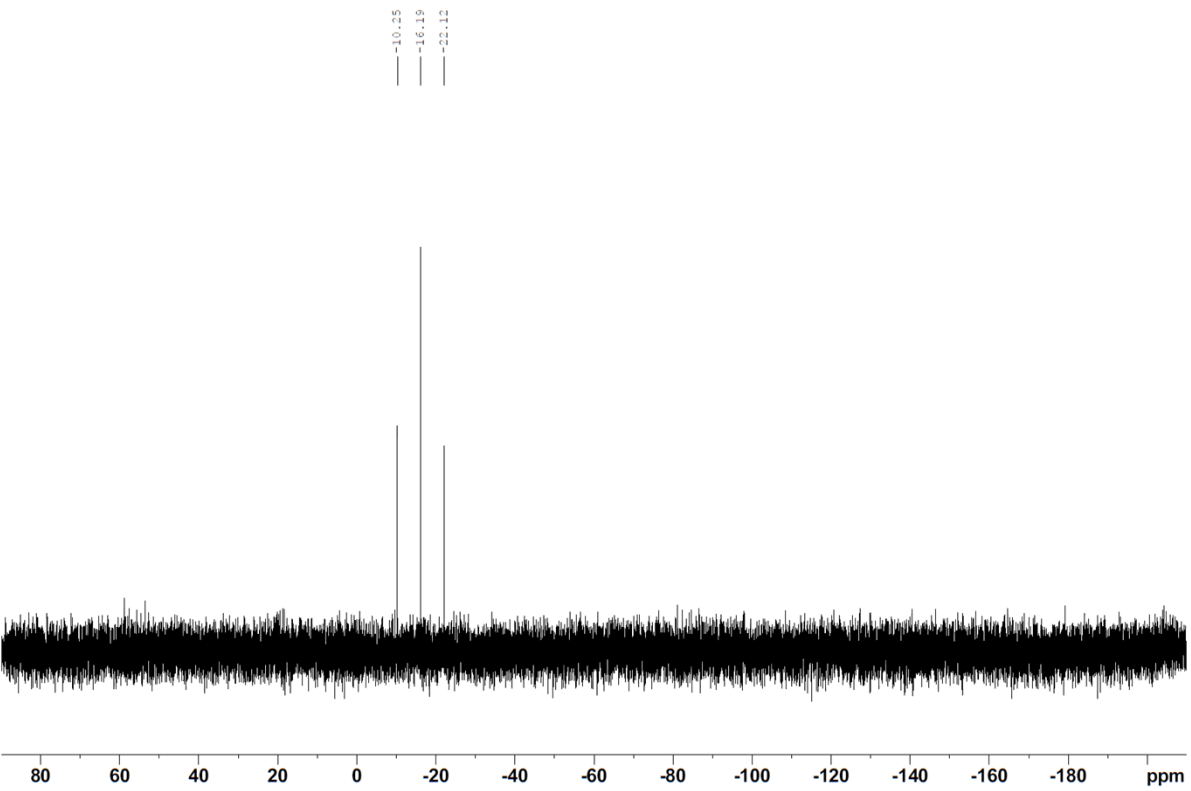

Figure S 24: $^{31}P\{^{1}H\}$ NMR spectrum of *fac*–[Re(κ^2–terpy)$(CO)_3(PO_2F_2)$], [**9**] in THF-d_8.

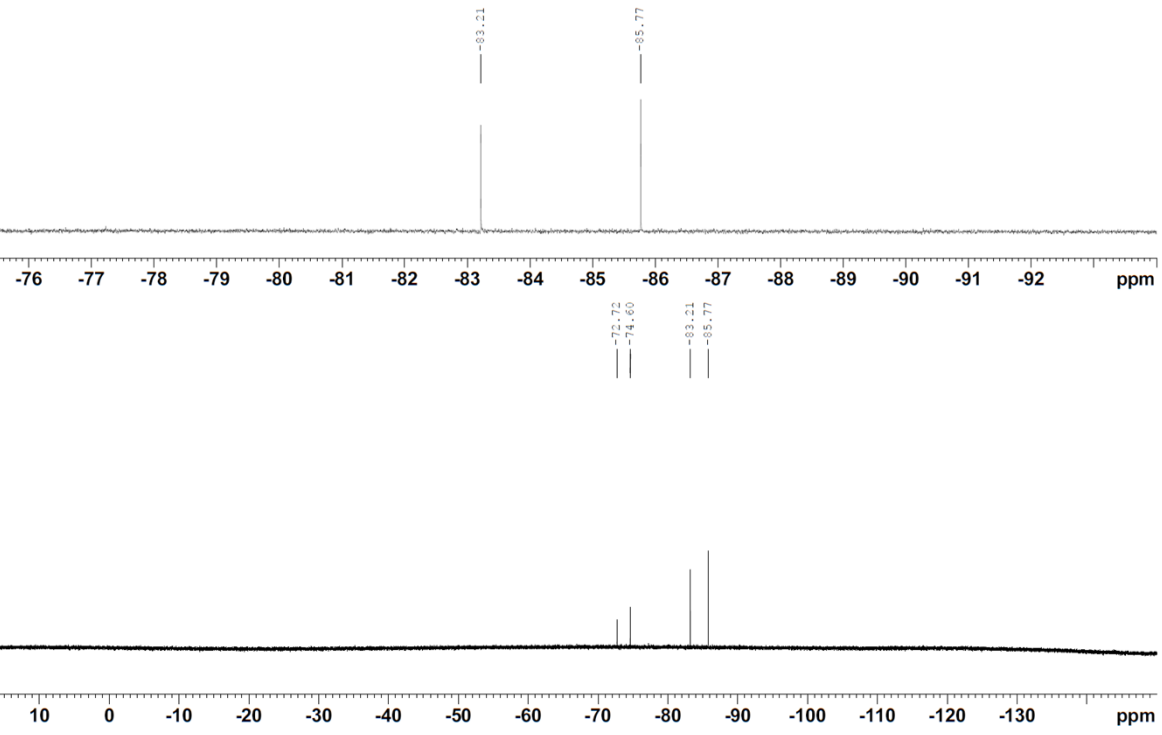

Figure S 25: $^{19}F\{^{1}H\}$ NMR spectrum of *fac*–[Re(κ^2–terpy)(CO)$_3$(PO_2F_2)], [**9**] in THF-d_8.

4.6 *fac*–[Re(κ^2–terpy)(CO)$_3$Br], [10]

Data in agreement with literature.[14]

4.7 *fac*–[Tc(κ²–terpy)(CO)₃Cl], [11]

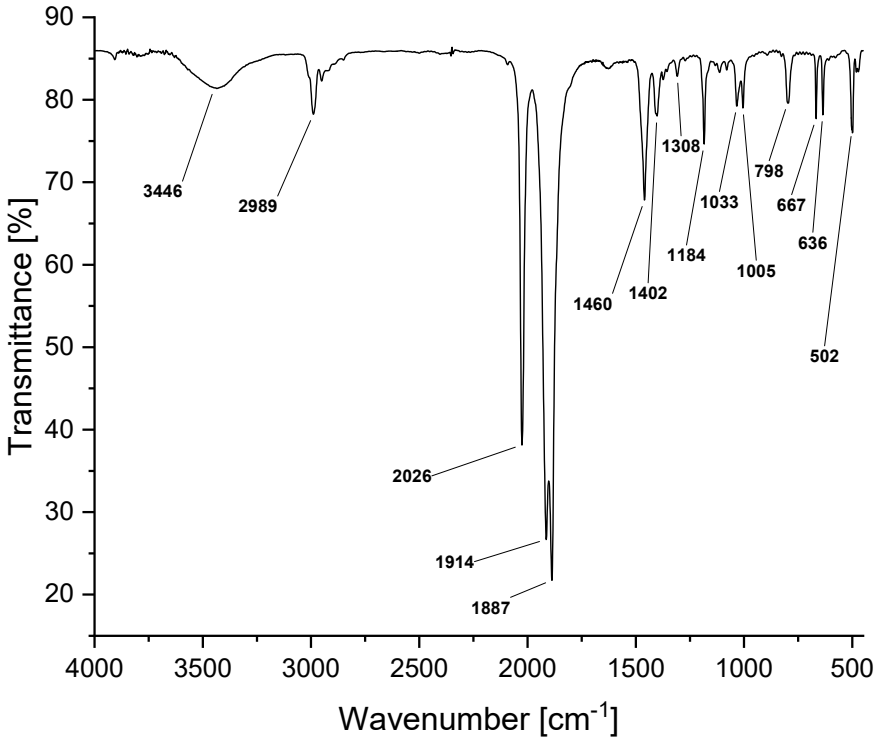

Figure S 26: IR spectrum (KBr) of *fac*–[Tc(κ²–terpy)(CO)₃Cl], [**11**].

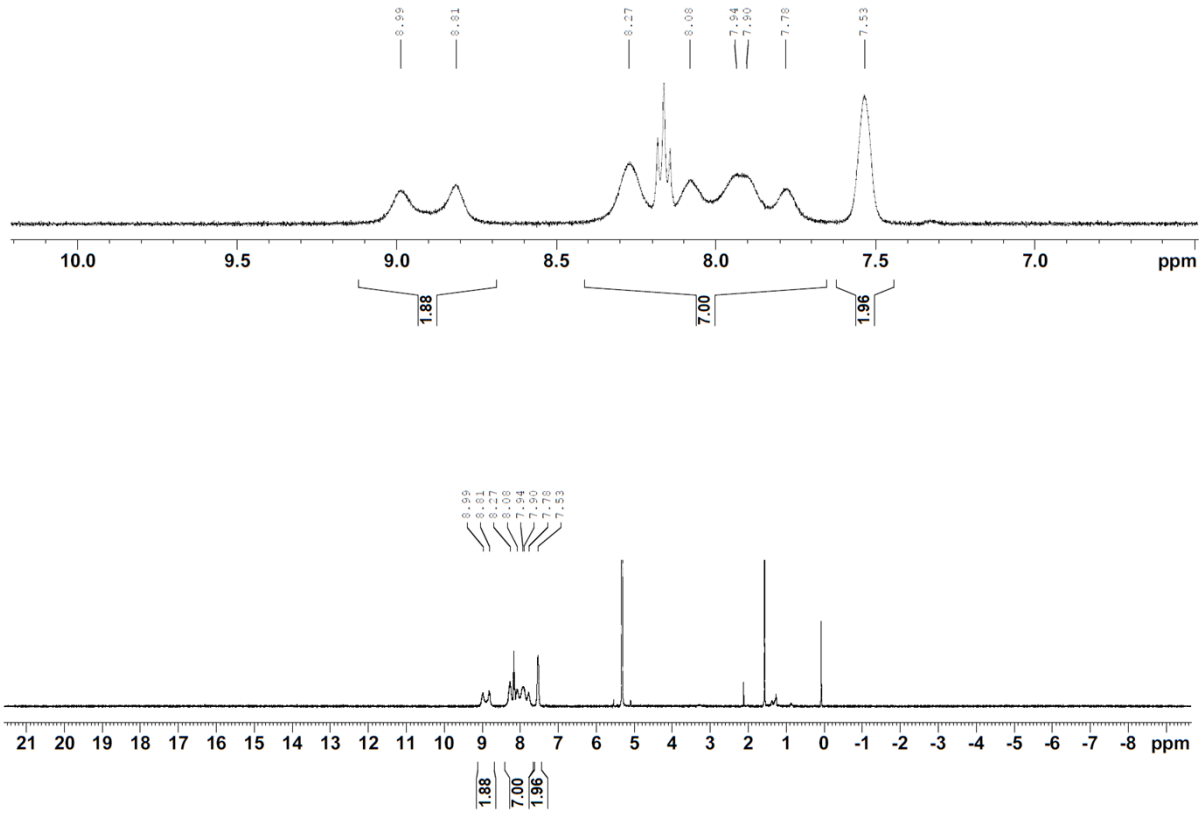

Figure S 27: ^{1}H NMR spectrum of *fac*–[Tc(κ^{2}–terpy)(CO)$_3$Cl], [**11**] at 298 K in CD_2Cl_2.

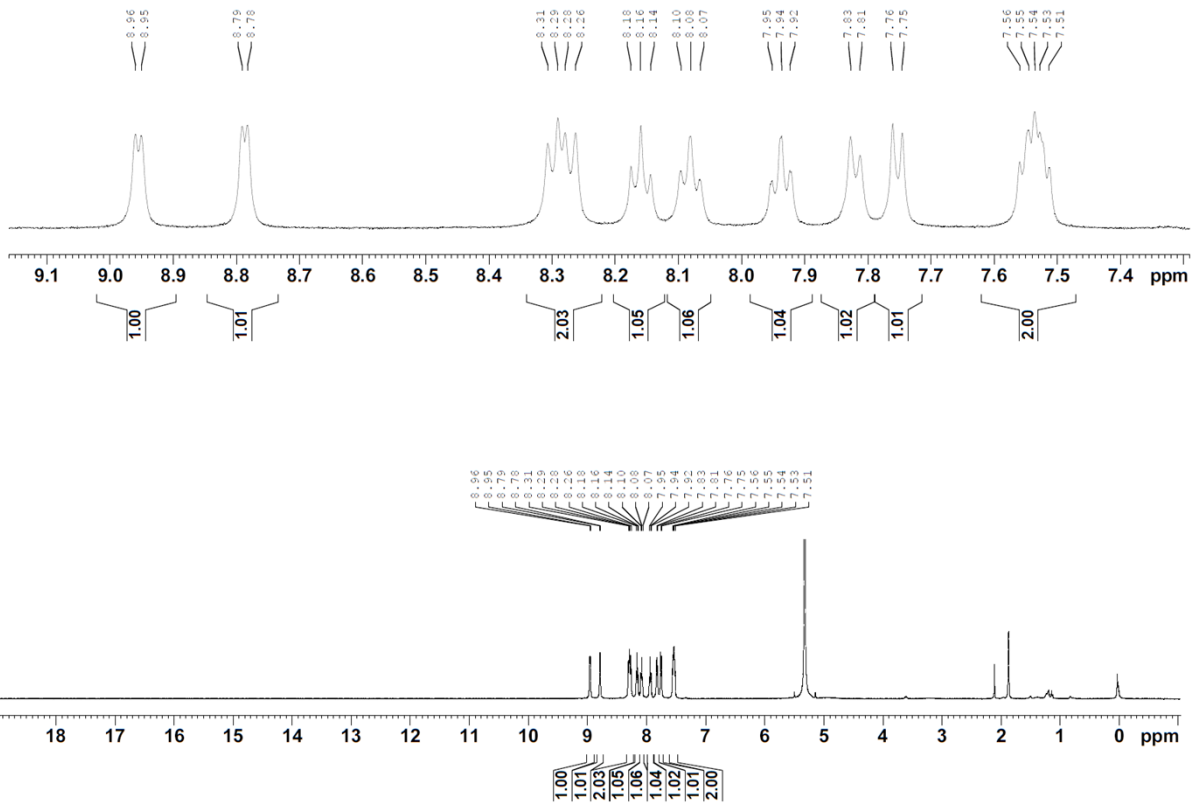

Figure S 28: ^{1}H NMR spectrum of *fac*–[Tc(κ^{2}–terpy)(CO)$_3$Cl], [**11**] at 235 K in CD_2Cl_2.

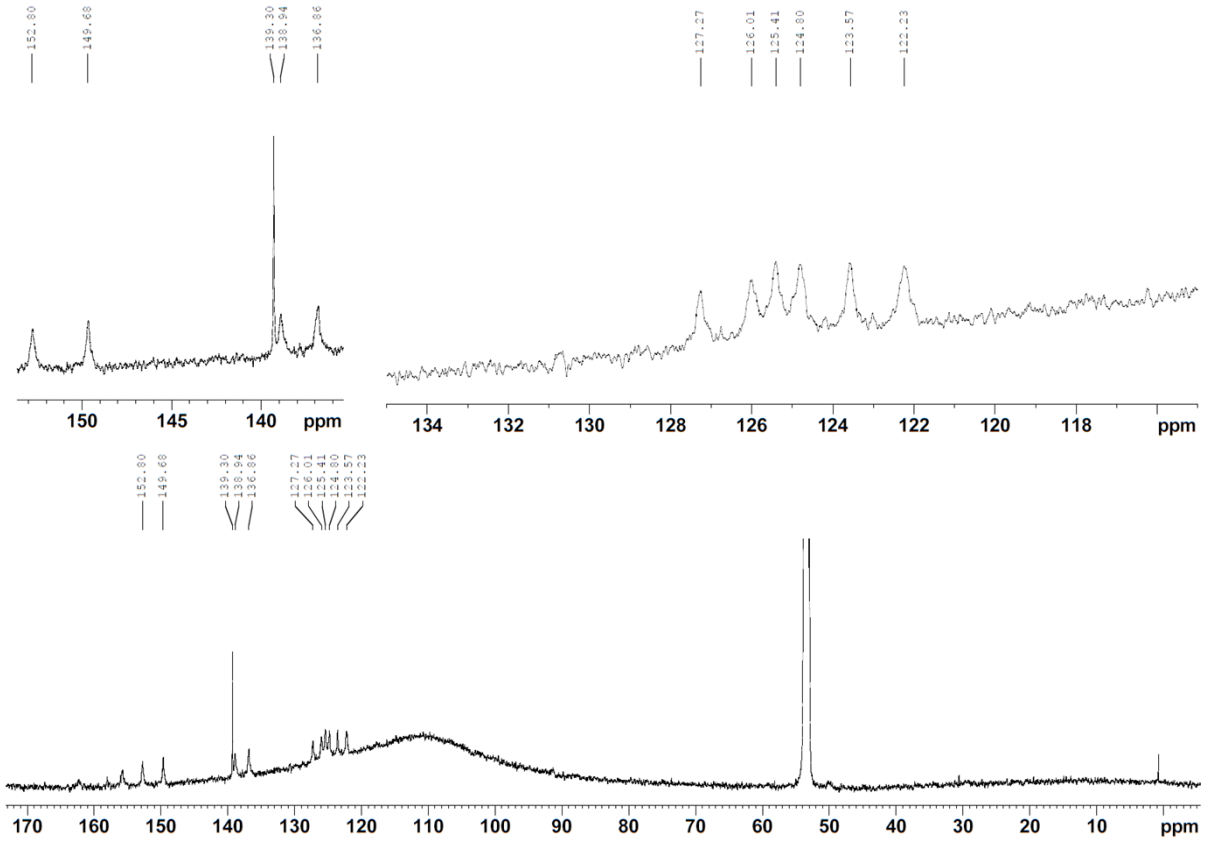

Figure S 29: $^{13}C\{^{1}H\}$ NMR spectrum of *fac*–[Tc(κ^2–terpy)(CO)$_3$Cl], [**11**] at 298 K in CD_2Cl_2.

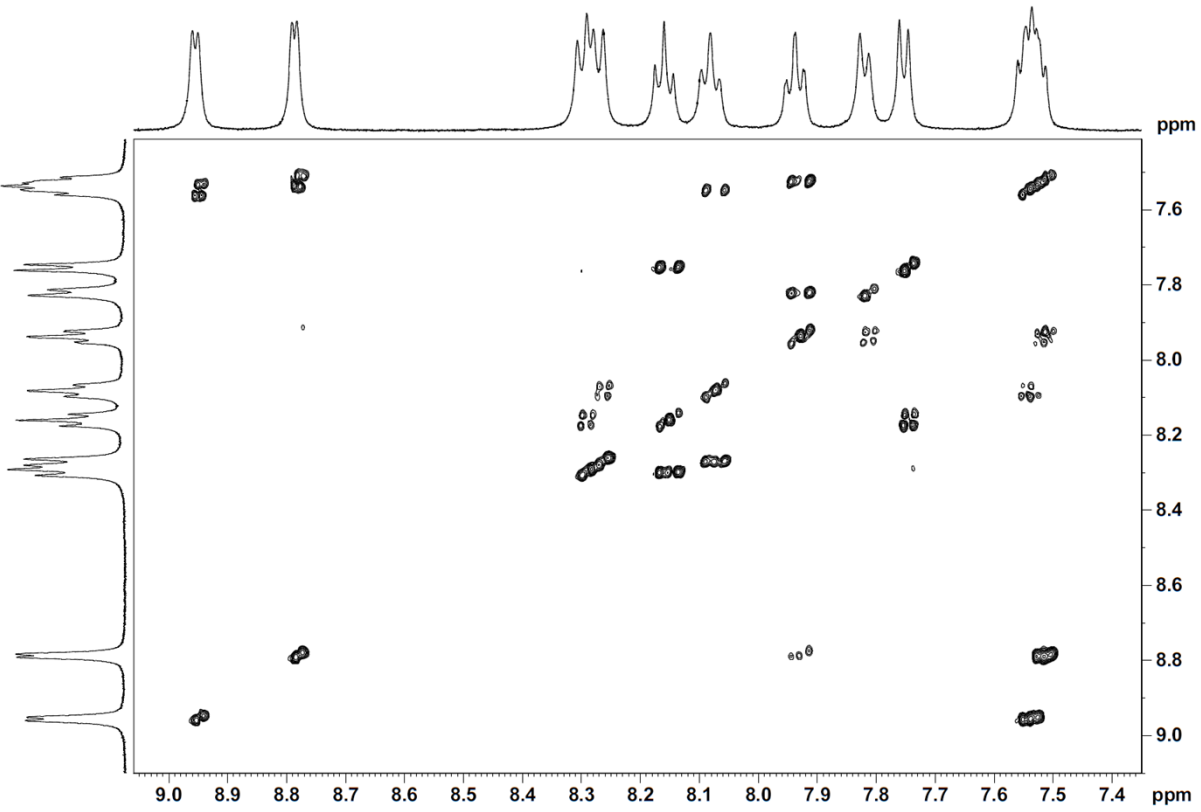

Figure S 30: ^{1}H–^{1}H COSY NMR spectrum of *fac*–[Tc(κ²–terpy)$(CO)_3$Cl], [**11**] at 235 K in CD_2Cl_2.

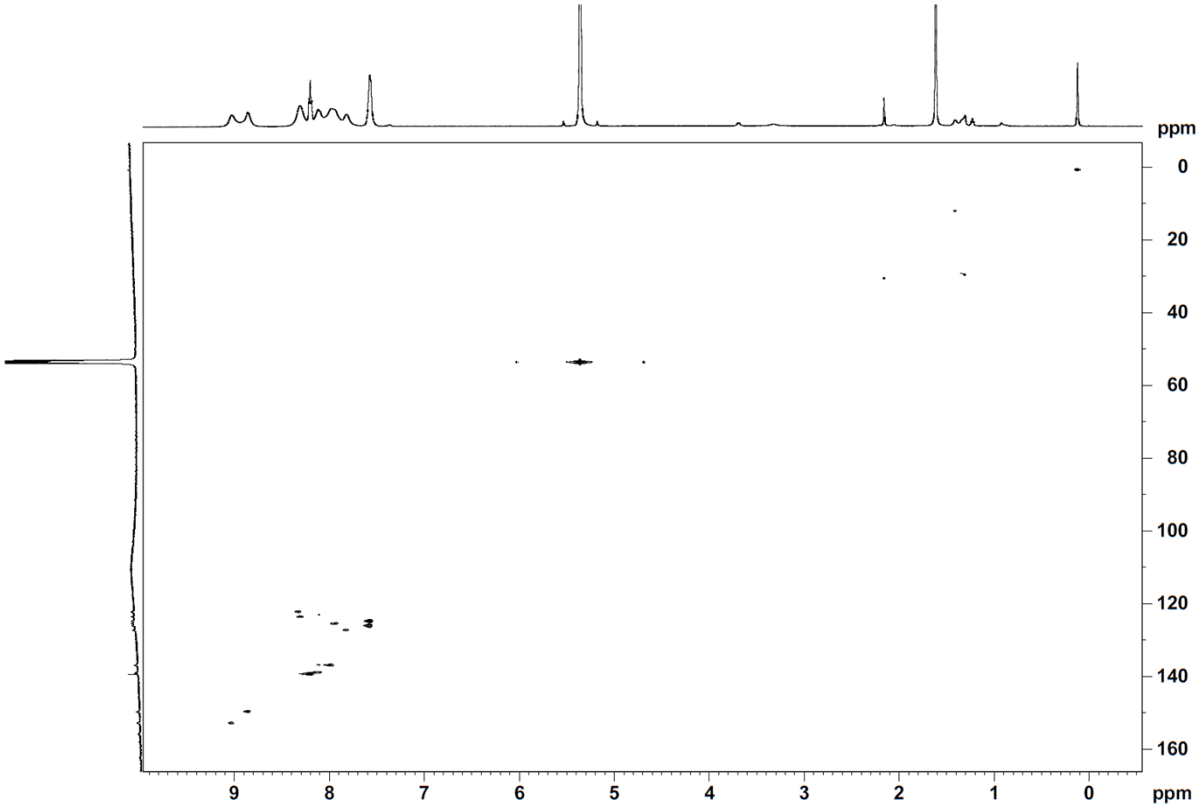

Figure S 31: $^{1}H–^{13}C$ HSQC NMR spectrum of *fac*–[Tc(κ^2–terpy)$(CO)_3Cl$], [**11**] at 298 K in CD_2Cl_2.

5 Crystallographic Data

CCDC entries 2307669-2307674 contain the supplementary crystallographic data for this paper. These data are provided free of charge by The Cambridge Crystallographic Data Centre *via* www.ccdc.cam.ac.uk/structures.

5.1 2,6-bis((di-tertbutylphosphino)methyl)pyridine ($^{Pyr}PNP^{tBu}$) (2)

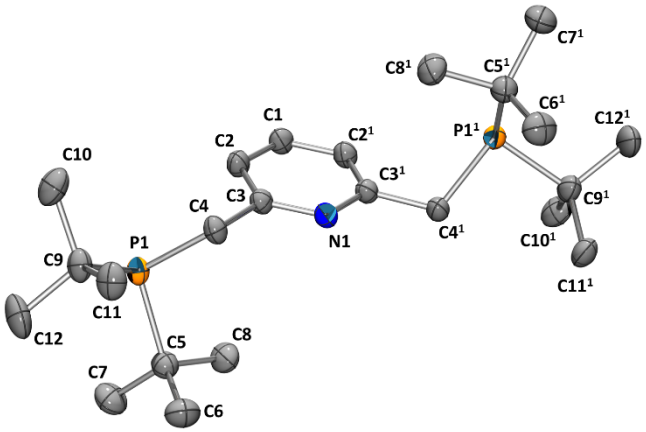

Figure S32: Ellipsoid displacement plot[15] of $^{Pyr}PNP^{tBu}$ (**2**). Ellipsoids represent 35% probability. Hydrogen atoms are omitted for clarity. Molecule has been prepared according to literature procedure (c.f. *General Experimental Details*).[5]

Table S1: Tabulated values of selected bond lengths and angles in the crystal structure of (**2**).

	Selected bond lengths		Selected bond angles
P1–C4	1.8611(16) Å	C4–P1–C5	102.50(8)°
P1–C5	1.8900(19) Å	C4–P1–C9	99.47(8)°
P1–C9	1.8891(18) Å	C5–P1–C9	110.92(9)°
N1–C3	1.3438(18) Å	C3–N1–C3^1	118.30(19)°
C1–C2	1.383(2) Å	C2–C1–C2^1	119.2(2)°
C2–C3	1.390(2) Å	N1–C3–C2	122.47(15)°
C3–C4	1.510(2) Å	C1–C2–C3	118.79(16)°

Table S2: Crystallographic data of $^{Pyr}PNP^{tBu}$ (**2**).

Empirical formula	$C_{23}H_{43}NP_2$
Formula weight	395.52
Diffractometer	*Rigaku* XtaLAB *Synergy, Dualflex*, HyPix
Radiation	CuKα (λ = 1.54184 Å)
Temperature [K]	160
Crystal system	monoclinic
Space group	C2/c
a [Å]	15.9398(4)
b [Å]	6.2656(2)
c [Å]	25.0585(8)
α [°]	90
β [°]	96.419(3)
γ [°]	90
Volume [Å3]	2486.96(13)
Z	4
ρ_{calc} [g/cm^3]	1.056
μ [mm^{-1}]	1.613
F(000)	872.0
Crystal size [mm^3]	0.125 × 0.08 × 0.071
Crystal description	clear, yellowish colorless block
2Θ range for data collection [°]	2.9 to 78.8
Index ranges	$-20 \leq h \leq 17$, $-7 \leq k \leq 7$, $-30 \leq l \leq 32$
Reflections collected	10581
Independent reflections	2652 [R_{int} = 0.0409, R_{sigma} = 0.0284]
Reflections observed	2456
Criterion for observation	I>2σ (I)
Completeness to theta	97.2% to 81.330°
Absorption correction	gaussian
Min./max. transmission	0.769/1.000
Data/restraints/parameters	2652/0/125
Goodness-of-fit on F^2	1.079
Final R indexes [I>=2σ (I)]	R_1 = 0.0563, wR_2 = 0.1482
Final R indexes [all data]	R_1 = 0.0583, wR_2 = 0.1508
Largest diff. peak/hole / [e Å^{-3}]	0.58/−0.46

5.2 *mer*–[Re(^{Pyr}PNP^{tBu})(CO)$_3$]$^+$, [**3**](PF$_6$)

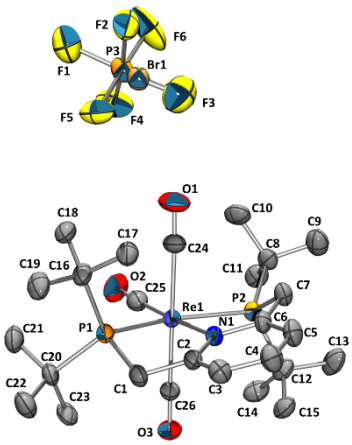

Figure S33: Ellipsoid displacement plot[15] of *mer*–[Re(^{Pyr}PNP^{tBu})(CO)$_3$](PF$_6$) ([**3**](PF$_6$)). Ellipsoids represent 35% probability. Hydrogen atoms are omitted for clarity.

Table S3: Tabulated values of selected bond lengths and angles in the crystal structure of [**3**](PF$_6$).

	Selected bond lengths		Selected bond angles
Re1–P1	2.4431(18) Å	P1–Re1–P2	159.03(7)°
Re1–P2	2.4565(17) Å	P1–Re1–N1	79.41(14)°
Re1–N1	2.215(5) Å	P2–Re1–N1	79.63(14)°
Re1–C24	2.017(8) Å	P1–Re1–C24	91.5(2)°
Re1–C25	1.921(11) Å	P1–Re1–C25	100.3(3)°
Re1–C26	1.998(7) Å	P1–Re1–C26	90.2(2)°
C24–O1	1.095(10) Å	C24–Re1–C25	87.9(4)°
C25–O2	1.163(12) Å	C25–Re1–C26	90.5(3)°
C26–O3	1.105(9) Å	C24–Re1–C26	177.9(3)°

Table S4: Crystallographic data of *mer*–[Re(^{Pyr}PNP^{tBu})(CO)$_3$](PF$_6$) ([**3**](PF$_6$)).

Empirical formula	$C_{26}H_{43}Br_{0.28}F_{4.34}NO_3P_{2.73}Re$
Formula weight	792.54
Diffractometer	Rigaku OD XtaLAB Synergy, Dualflex, Pilatus 200K
Radiation	CuKα (λ = 1.54184 Å)
Temperature [K]	160
Crystal system	triclinic
Space group	$P\bar{1}$
a [Å]	8.4694 (2)
b [Å]	12.7901 (2)
c [Å]	15.8962 (3)
α [°]	105.675(2)
β [°]	104.744(2)
γ [°]	92.815(2)
Volume [Å3]	1590.42 (6)
Z	2
ρ_{calc} [g/cm^3]	1.655
μ [mm^{-1}]	9.636
F(000)	789.0
Crystal size [mm^3]	0.068 × 0.047 × 0.021
Crystal description	plate, yellowish
2Θ range for data collection [°]	6.012 to 159.956
Index ranges	$-10 \le h \le 10$, $-16 \le k \le 16$, $-20 \le l \le 20$
Reflections collected	57628
Independent reflections	6827 [R_{int} = 0.0817, R_{sigma} = 0.0316]
Reflections observed	6199
Criterion for observation	I>2σ (I)
Completeness to theta	98.3% to 79.978°
Absorption correction	gaussian
Min./max. transmission	0.484/0.845
Data/restraints/parameters	6827/12/384
Goodness-of-fit on F^2	1.082
Final R indexes [I>=2σ (I)]	R_1 = 0.0558, wR_2 = 0.1477
Final R indexes [all data]	R_1 = 0.0609, wR_2 = 0.1523
Largest diff. peak/hole / [e Å^{-3}]	1.54/−2.98

Note: The PF_6^- counterion is disordered with Br^- at an occupancy of 0.28.

5.3 *mer*–[Re(^{Pyr}PNP^{tBu})(CO)$_3$]$^+$, [3](BF$_4$)

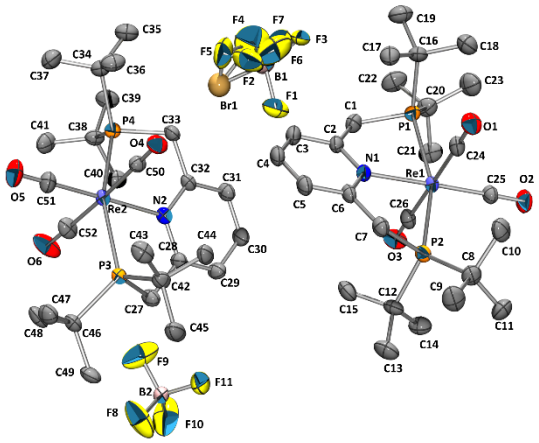

Figure S34: Ellipsoid displacement plot[15] of *mer*–[Re(^{Pyr}PNP^{tBu})(CO)$_3$](BF$_4$) ([**3**](BF$_4$)). Ellipsoids represent 35% probability. Hydrogen atoms are omitted for clarity.

Table S5: Tabulated values of selected bond lengths and angles in the crystal structure of [**3**](BF$_4$).

	Selected bond lengths		Selected bond angles
Re1–P1	2.4454(12) Å	P1–Re1–P2	158.30(4)°
Re1–P2	2.4477(12) Å	P1–Re1–N1	79.28(11)°
Re1–N1	2.200(4) Å	P2–Re1–N1	79.03(11)°
Re1–C24	2.004(5) Å	P1–Re1–C24	90.82(16)°
Re1–C25	1.925(5) Å	P1–Re1–C25	100.88(16)°
Re1–C26	1.975(5) Å	P1–Re1–C26	88.12(16)°
C24–O1	1.117(7) Å	C24–Re1–C25	90.3(2)°
C25–O2	1.140(6) Å	C25–Re1–C26	89.8(2)°
C26–O3	1.145(6) Å	C24–Re1–C26	178.9(2)°

Table S6: Crystallographic data of *mer*–[Re(^{Pyr}PNP^{tBu})(CO)$_3$](BF$_4$) ([**3**](BF$_4$)).

Empirical formula	$C_{52}H_{86}B_{1.95}Br_{0.05}F_{7.8}N_2O_6P_4Re_2$
Formula weight	1504.78
Diffractometer	Rigaku OD XtaLAB Synergy, Dualflex, Pilatus 200K
Radiation	CuKα (λ = 1.54184 Å)
Temperature [K]	160
Crystal system	triclinic
Space group	$P\bar{1}$
a [Å]	8.87921 (7)
b [Å]	12.57039 (13)
c [Å]	27.5441 (2)
α [°]	85.4844 (7)
β [°]	89.7211 (6)
γ [°]	89.6147 (8)
Volume [Å3]	3064.69 (5)
Z	2
ρ_{calc} [g/cm^3]	1.631
μ [mm^{-1}]	9.226
F(000)	1503.0
Crystal size [mm^3]	0.082 × 0.072 × 0.035
Crystal description	plate, yellow
2Θ range for data collection [°]	6.438 to 159.324
Index ranges	$-11 \leq h \leq 11$, $-15 \leq k \leq 15$, $-35 \leq l \leq 34$
Reflections collected	81167
Independent reflections	12861 [R_{int} = 0.0586, R_{sigma} = 0.0286]
Reflections observed	11547
Criterion for observation	I>2σ (I)
Completeness to theta	99.6% to 79.662°
Absorption correction	gaussian
Min./max. transmission	0.270/0.698
Data/restraints/parameters	12861/48/740
Goodness-of-fit on F^2	1.086
Final R indexes [I>=2σ (I)]	R_1 = 0.0383, wR_2 = 0.1040
Final R indexes [all data]	R_1 = 0.0420, wR_2 = 0.1063
Largest diff. peak/hole / [e Å^{-3}]	1.14/−2.39

Note: One of the BF_4^- counterions is disordered with Br^- at an occupancy of 0.05.

5.4 *mer*–[Tc(^{Pyr}PNP^{tBu})(CO)$_3$]$^+$, [5](PF$_6$)

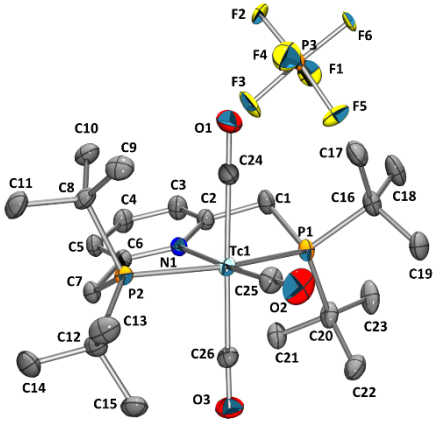

Figure S35: Ellipsoid displacement plot[15] of *mer*–[Tc(^{Pyr}PNP^{tBu})(CO)$_3$](PF$_6$) ([**5**](PF$_6$)). Ellipsoids represent 35% probability. Hydrogen atoms are omitted for clarity.

Table S7: Tabulated values of selected bond lengths and angles in the crystal structure of [**5**](PF$_6$).

	Selected bond lengths		Selected bond angles
Tc1–P1	2.4578(10) Å	P1–Tc1–P2	159.76(4)°
Tc1–P2	2.4495(10) Å	P1–Tc1–N1	80.02(9)°
Tc1–N1	2.206(3) Å	P2–Tc1–N1	79.75(9)°
Tc1–C24	1.993(5) Å	P1–Tc1–C24	88.34(14)°
Tc1–C25	1.917(5) Å	P1–Tc1–C25	100.76(16)°
Tc1–C26	1.988(5) Å	P1–Tc1–C26	90.68(13)°
C24–O1	1.118(6) Å	C24–Tc1–C25	88.2(2)°
C25–O2	1.144(6) Å	C25–Tc1–C26	90.6(2)°
C26–O3	1.122(6) Å	C24–Tc1–C26	178.35(18)°

Table S8: Crystallographic data of *mer*–[Tc(^{Pyr}PNP^{tBu})(CO)$_3$](PF$_6$) ([**5**](PF$_6$)).

Empirical formula	$C_{26}H_{43}Cl_{0.4}F_{3.6}NO_3P_{2.6}Tc$
Formula weight	678.71
Diffractometer	Rigaku OD XtaLAB Synergy, Dualflex, Pilatus 200K
Radiation	CuKα (λ = 1.54184 Å)
Temperature [K]	160
Crystal system	triclinic
Space group	$P\bar{1}$
a [Å]	8.38590 (10)
b [Å]	12.89050 (10)
c [Å]	15.67840 (10)
α [°]	106.0060 (10)
β [°]	103.6810 (10)
γ [°]	92.6590 (10)
Volume [Å3]	1571.54 (3)
Z	2
ρ_{calc} [g/cm^3]	1.434
μ [mm^{-1}]	5.705
F(000)	702.0
Crystal size [mm^3]	0.13 × 0.096 × 0.041
Crystal description	plate, yellow
2Θ range for data collection [°]	6.072 to 158.478
Index ranges	$-10 \leq h \leq 10$, $-16 \leq k \leq 16$, $-18 \leq l \leq 19$
Reflections collected	63888
Independent reflections	6773 [R_{int} = 0.0556, R_{sigma} = 0.0201]
Reflections observed	6637
Criterion for observation	I>2σ (I)
Completeness to theta	99.9% to 79.239°
Absorption correction	gaussian
Min./max. transmission	0.700/1.000
Data/restraints/parameters	6773/4/377
Goodness-of-fit on F^2	1.056
Final R indexes [I>=2σ (I)]	R_1 = 0.0555, wR_2 = 0.1747
Final R indexes [all data]	R_1 = 0.0560, wR_2 = 0.1753
Largest diff. peak/hole / [e Å^{-3}]	2.83/−1.08

Note: The PF_6^- counterion is disordered with Cl^- at an occupancy of 0.40, omitted in Figure S35.

5.5 *fac*–[Re(κ²–terpy)(CO)$_3$(PO$_2$F$_2$)], [9]

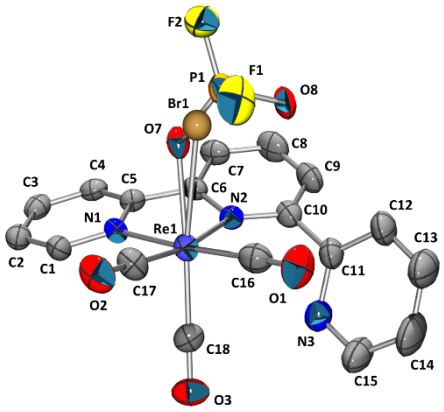

Figure S36: Ellipsoid displacement plot[15] of *fac*–[Re(κ²–terpy)(CO)$_3$(PO$_2$F$_2$)] [**9**]. Ellipsoids represent 35% probability. Hydrogen atoms are omitted for clarity. The unit cell contains both the shown isomer, while the second isomer is omitted for clarity.

Table S9: Tabulated values of selected bond lengths and angles in the crystal structure of [**9**].

	Selected bond lengths		Selected bond angles
Re1–N1	2.165(5) Å	N1–Re1–N2	74.98(19)°
Re1–N2	2.215(5) Å	N1–Re1–C16	175.5(3)°
Re1–C16	1.915(9) Å	N1–Re1–C17	96.5(3)°
Re1–C17	1.906(7) Å	N1–Re1–C18	94.5(3)°
Re1–C18	1.900(8) Å	N1–Re1–O7	79.6(2)°
Re1–O7	2.167(6) Å	O7–P1–O8	108.8(3)°
C16–O1	1.169(10) Å	C16–Re1–C17	87.3(3)°
C17–O2	1.146(9) Å	C17–Re1–C18	88.7(3)°
C18–O3	1.142(9) Å	C16–Re1–C18	88.1(3)°

Table S10: Crystallographic data of *fac*–[Re(κ²–terpy)(CO)$_3$(PO_2F_2)] [**9**].

Empirical formula	$C_{36}H_{22}Br_{0.26}F_{3.48}N_6O_{9.48}P_{1.74}Re_2$
Formula weight	678.71
Diffractometer	Rigaku OD XtaLAB Synergy, Dualflex, Pilatus 200K
Radiation	CuKα (λ = 1.54184 Å)
Temperature [K]	160
Crystal system	triclinic
Space group	$P\bar{1}$
a [Å]	8.4380 (2)
b [Å]	9.6908 (2)
c [Å]	27.1602 (4)
α [°]	96.4300 (10)
β [°]	97.0310 (10)
γ [°]	104.920 (2)
Volume [Å3]	2105.92 (8)
Z	2
ρ_{calc} [g/cm^3]	1.898
μ [mm^{-1}]	12.643
F(000)	1145.0
Crystal size [mm^3]	0.12 × 0.072 × 0.018
Crystal description	plate, yellow
2Θ range for data collection [°]	6.632 to 147.798
Index ranges	$-10 \le h \le 10$, $-11 \le k \le 12$, $-33 \le l \le 31$
Reflections collected	53308
Independent reflections	8152 [R_{int} = 0.0663, R_{sigma} = 0.0276]
Reflections observed	7569
Criterion for observation	I>2σ (I)
Completeness to theta	99.8% to 73.899°
Absorption correction	gaussian
Min./max. transmission	0.535/1.000
Data/restraints/parameters	8152/1/551
Goodness-of-fit on F^2	1.074
Final R indexes [I>=2σ (I)]	R_1 = 0.0415, wR_2 = 0.1047
Final R indexes [all data]	R_1 = 0.0442, wR_2 = 0.1066
Largest diff. peak/hole / [e Å^{-3}]	1.33/−2.64

Note: The unit cell contains both isomers, but only one is shown in Figure S36. The $PO_2F_2^-$ counterion is disordered with Br^- at an occupancy of 0.13.

5.6 *fac*–[Tc(κ²–terpy)(CO)₃Cl], [11]

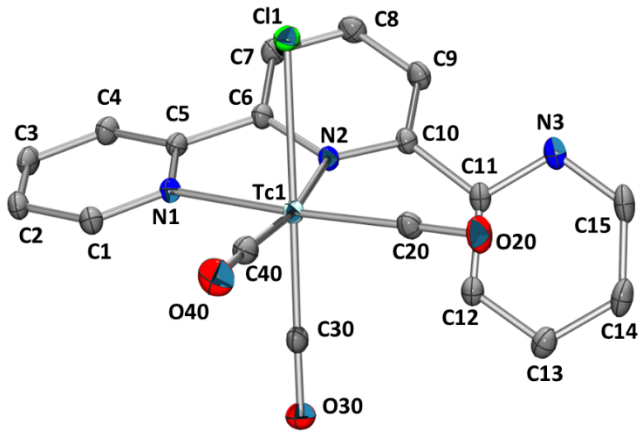

Figure S37: Ellipsoid displacement plot[15] of *fac*–[Tc(κ²–terpy)(CO)₃Cl] [**11**]. Ellipsoids represent 35% probability. Hydrogen atoms are omitted for clarity.

Table S11: Tabulated values of selected bond lengths and angles in the crystal structure of [**11**].

	Selected bond lengths		Selected bond angles
Tc1–N1	2.1779(12) Å	N1–Tc1–N2	75.09(5)°
Tc1–N2	2.2378(12) Å	N1–Tc1–C20	175.97(5)°
Tc1–C20	1.9248(16) Å	N1–Tc1–C30	92.80(5)°
Tc1–C30	1.8901(16) Å	N1–Tc1–C40	97.72(6)°
Tc1–C40	1.9124(16) Å	N1–Tc1–Cl1	85.99(3)°
Tc1–Cl1	2.5040(4) Å	N2–Tc1–Cl1	82.53(3)°
C20–O20	1.1453(19) Å	C20–Tc1–C30	89.10(6)°
C30–O30	1.146(2) Å	C30–Tc1–C40	88.32(7)°
C40–O40	1.143(2) Å	C20–Tc1–C40	85.88(7)°

Table S12: Crystallographic data of *fac*–[Tc(κ²–terpy)(CO)$_3$Cl)] [**11**].

Empirical formula	$C_{18}H_{11}ClN_3O_3Tc$
Formula weight	450.75
Diffractometer	*Rigaku* XtaLAB *Synergy, Dualflex*, HyPix
Radiation	MoKα (λ = 0.71073 Å)
Temperature [K]	160
Crystal system	monoclinic
Space group	$I2/_a$
a [Å]	16.6643 (3)
b [Å]	7.04490 (10)
c [Å]	29.6513 (6)
α [°]	90
β [°]	102.168 (2)
γ [°]	90
Volume [Å3]	3402.81 (11)
Z	8
ρ_{calc} [g/cm^3]	1.760
μ [mm^{-1}]	1.027
F(000)	1792.0
Crystal size [mm^3]	0.57 × 0.41 × 0.1
Crystal description	plate, green
2Θ range for data collection [°]	5.002 to 59.144
Index ranges	$-21 \le h \le 21$, $-9 \le k \le 9$, $-40 \le l \le 36$
Reflections collected	24908
Independent reflections	4254 [R_{int} = 0.0221, R_{sigma} = 0.0157]
Reflections observed	4032
Criterion for observation	I>2σ (I)
Completeness to theta	99.9% to 29.6630°
Absorption correction	gaussian
Min./max. transmission	0.224/1.000
Data/restraints/parameters	4254/0/235
Goodness-of-fit on F^2	1.069
Final R indexes [I>=2σ (I)]	R_1 = 0.0190, wR_2 = 0.0473
Final R indexes [all data]	R_1 = 0.0204, wR_2 = 0.0479
Largest diff. peak/hole / [e Å^{-3}]	0.51/−0.37

6. References

[1] R. Alberto, R. Schibli, A. Egli, A. P. Schubiger, U. Abram, T. A. Kaden, *J. Am. Chem. Soc.* **1998**, *120*, 7987–7988.

[2] R. Lengacher, Y. Wang, H. Braband, O. Blacque, G. Gasser, R. Alberto, *Chem. Commun.* **2021**, *57*, 13349–13352.

[3] R. Alberto, A. Egli, U. Abram, K. Hegetschweiler, V. Gramlich, A. P. Schubiger, *J. Chem. Soc. Dalt. Trans.* **1994**, 2815–2820.

[4] R. Alberto, R. Schibli, A. Egli, W. A. Herrmann, G. Artus, U. Abram, T. A. Kaden, *J. Organomet. Chem.* **1995**, *492*, 217–224.

[5] Z. Li, T. M. Rayder, L. Luo, J. A. Byers, C. K. Tsung, *J. Am. Chem. Soc.* **2018**, *140*, 8082–8085.

[6] R. C. Clark, J. S. Reid, *Acta Crystallogr. Sect. A* **1995**, *51*, 887–897.

[7] "CrysAlisPro (version 1.171.40.68a), Rigaku Oxford Diffraction," **2019**.

[8] O. V. Dolomanov, L. J. Bourhis, R. J. Gildea, J. A. K. Howard, H. Puschmann, *J. Appl. Crystallogr.* **2009**, *42*, 339–341.

[9] G. M. Sheldrick, *Acta Crystallogr. Sect. A* **2015**, *71*, 3–8.

[10] G. M. Sheldrick, *Acta Crystallogr. Sect. C* **2015**, *71*, 3–8.

[11] A. L. Spek, *Acta Crystallogr. Sect. C* **2015**, *71*, 9–18.

[12] M. L. Besmer, H. Braband, T. Fox, B. Spingler, A. P. Sattelberger, R. Alberto, *Inorg. Chem.* **2023**, *62*, 10727–10735.

[13] H.-O. Kalinowski, S. Berger, S. Braun, *13C-NMR-Spektroskopie*, Thieme, New York, **1984**.

[14] E. W. Abel, V. S. Dimitrov, N. J. Long, K. G. Orrell, A. G. Osborne, H. M. Pain, V. Sik, M. B. Hursthouse, M. A. Mazidc, *J. Chem. Soc. Dalt. Trans.* **1993**, 597–603.

[15] L. J. Farrugia, *J. Appl. Crystallogr.* **1997**, *30*, 565–565.